**Atmospheric
Chemistry
and Physics**

Modelling the impacts of ammonia emissions reductions on North American air quality

P. A. Makar[1], M. D. Moran[1], Q. Zheng[1], S. Cousineau[2], M. Sassi[2], A. Duhamel[2], M. Besner[2], D. Davignon[2], L.-P. Crevier[2], and V. S. Bouchet[2]

[1]Air Quality Research Division, Science and Technology Branch, Environment Canada, Toronto, Ontario, Canada
[2]Air Quality Model Applications Section, Meteorological Service of Canada, Environment Canada, Montreal, Quebec, Canada

Abstract. A unified regional air-quality modelling system (AURAMS) was used to investigate the effects of reductions in ammonia emissions on regional air quality, with a focus on particulate-matter formation. Three simulations of one-year duration were performed for a North American domain: (1) a base-case simulation using 2002 Canadian and US national emissions inventories augmented by a more detailed Canadian emissions inventory for agricultural ammonia; (2) a 30% North-American-wide reduction in agricultural ammonia emissions; and (3) a 50% reduction in Canadian beef-cattle ammonia emissions. The simulations show that a 30% continent-wide reduction in agricultural ammonia emissions lead to reductions in median hourly $PM_{2.5}$ mass of $<1\,\mu g\,m^{-3}$ on an annual basis. The atmospheric response to these emission reductions displays marked seasonal variations, and on even shorter time scales, the impacts of the emissions reductions are highly episodic: 95th-percentile hourly $PM_{2.5}$ mass decreases can be up to a factor of six larger than the median values.

A key finding of the modelling work is the linkage between gas and aqueous chemistry and transport; reductions in ammonia emissions affect gaseous ammonia concentrations close to the emissions site, but substantial impacts on particulate matter and atmospheric deposition often occur at considerable distances downwind, with particle nitrate being the main vector of ammonia/um transport. Ammonia emissions reductions therefore have trans-boundary consequences downwind. Calculations of critical-load exceedances for sensitive ecosystems in Canada suggest that ammonia emission reductions will have a minimal impact on current ecosystem acidification within Canada, but may have a substantial impact on future ecosystem acidification. The 50% Canadian beef-cattle ammonia emissions reduction scenario was used to examine model sensitivity to uncertainties in the new Canadian agricultural ammonia emissions inventory, and the simulation results suggest that further work is needed to improve the emissions inventory for this particular sector. It should be noted that the model in its current form neglects coarse mode base cation chemistry, so the predicted effects of ammonia emissions reductions shown here should be considered upper limits.

1 Introduction

The chemistry describing the interactions of atmospheric ammonia (NH_3) with other atmospheric constituents has been well established through field and laboratory studies. While very high concentrations of ammonia gas are known to have health impacts (e.g., Stilg, 1994), its role in the creation of airborne particulate matter (PM) at lower concentrations is of interest due to the known effects of fine particulate matter on human health (cf. Schwarze et al., 2006).

The creation of airborne PM from ammonia is dependant on the presence of other precursor gases, primarily directly-emitted sulphur dioxide and nitrogen oxides (SO_2 and NO_x; Seinfeld and Pandis, 1998). SO_2 may oxidize via gas-phase (Stockwell and Calvert, 1983) and/or aqueous-phase (Coste and Courtier, 1936; Junge and Ryan, 1958; Hermann et al., 2000, 2005) reactions, creating sulphuric acid gas or sulphuric acid ions in cloud or rain water, respectively. The vapour pressure of sulphuric acid gas is sufficiently low that almost all of the gas created will partition to the particle phase, either through condensation on existing particles or

nucleation of new particles. Sulphuric acid created in cloud and/or rainwater may be transferred to the particle phase upon droplet evaporation.

Ammonia affects aqueous-phase chemistry through the provision of a weak base; the hydrogen ion concentration will be inversely proportional to the ammonia partial pressure. Reductions in the hydrogen ion concentration due to excess ammonia will allow a greater aqueous uptake of SO_2 in cloud water in the form of the bisulphite ion (HSO_3^-). The latter may be oxidized by hydrogen peroxide, ozone, organic peroxides, or catalytic oxygen reactions to bisulphate and sulphate ions, the ionic equilibrium products of sulphuric acid dissociation (Hermann et al., 2000, 2005). H_2O_2 is believed to be the dominant aqueous-phase oxidant of HSO_3^-, but the strongly pH-dependent oxidation by O_3 becomes more important as pH increases or when H_2O_2 has been depleted (e.g., Fung et al., 1991). The relative contribution of these two oxidants to aqueous-phase sulphate formation is therefore influenced by NH_3 levels. An additional process of importance for ammonia chemistry is the formation of gaseous nitric acid (HNO_3) through well-known "NO_x termination" reactions (Seinfeld and Pandis, 1998); HNO_3 may in turn participate in aqueous reactions with the ammonium ion, or in particle-phase chemistry.

Laboratory studies and related thermodynamics of high-concentration particle ammonium chemistry are well established (cf. D'Ans, 1913), and observations of ammonium, sulphate, and nitrate in PM have appeared in the literature over the past sixty years (cf. Robbins and Cadle, 1958; Fenn et al., 1963; Spurny and Heard, 1969; Heard and Wiffen, 1969; Gordon and Bryan, 1973; Anlauf et al., 1978; Brosset, 1978; Stelson et al., 1979; Tanner, 1983). The partitioning between different phases, including gases, may be predicted using fundamental thermodynamics theory (cf. Kusik and Meissner, 1978) in box models (e.g., Ansari and Pandis, 1999; Makar et al., 2003) or regional models such as AURAMS (Gong et al., 2006).

The concept of ammonia limitation has been used in the past (Blanchard et al., 1999), in order to better understand the aqueous and particulate chemistry of ammonia. By analogy to the NO_x- and VOC-limit concept for ozone formation, which refer to environments in which changes in NO_x or VOC emissions respectively have the greatest impact on changes in the ozone concentration, ammonia limitation refers to the thermodynamic conditions (a chemical *regime*) in which changes to ammonia emissions have a significant impact on particle mass. Specifically, an *ammonia-limited* regime is one in which the total available ammonia (gaseous ammonia + aerosol phase ammonium) is insufficient to charge-balance difference the remaining other anions and cations (cf. Blanchard et al., 1999), with the result that small perturbations in the ammonia emissions may have a significant effect on particle mass. Ammonia-limited regimes are thus those in which:

$$[NH_3(g)] + [NH_4^+(aq)] < \left\{ 2[Ca^{2+}] + 2[Mg^{2+}] + [Na^+] + [K^+] \right. \tag{1}$$
$$\left. - 2[SO_4^{2-}(aq)] - [NO_3^-(aq)] - [HNO_3(g)] - [HCl(g)] - [Cl^-(aq)] \right\}$$

The above equation is appropriate for bulk chemistry in which all species are in a common mixture. The ionic species in the above equation refer to all forms of the species in particles and cloud water. In the ambient atmosphere, the situation is complicated by the size segregation of some of the cations and anions into different particle size modes in the overall particle size distribution. Calcium, magnesium, sodium and potassium base cations all typically have the greatest portion of their mass in the coarse mode (particle sizes greater than 2.5 μm aerodynamic diameter), since their dominant sources are in soil dust, and sea- or road-salt. Most the sulphate mass is produced from sulphur dioxide oxidation by cloud water aqueous-phase reactions or gas-phase hydroxyl radical reaction, both of which create sulphuric acid. This, in turn forms particle sulphate with a mass peak in smaller particles (less than 2.5 μm diameter) due to nucleation, condensation and cloud evaporation processes favouring the smaller sizes.

Equation (1) suggests that total ammonia will have little effect on particle formation if large amounts of calcium, magnesium, sodium or potassium are present. The size segregation of sulphate from these cations, however, suggests that a two equation definition would more closely describe the impact of ammonia in the ambient atmosphere:

$$[NH_3(g)] + [NH_4^+(aq)] < 2[SO_4^{2-}(aq)], \text{ and} \tag{2a}$$

$$[NH_3(g)] + [NH_4^+(aq)] - 2[SO_4^{2-}(aq)] < \tag{2b}$$
$$\left\{ [NO_3^-(aq)] + [HNO_3(g)] + [HCl(g)] + [Cl^-(aq)] \right.$$
$$\left. - 2[Ca^{2+}] - 2[Mg^{2+}] - [Na^+] - [K^+] \right\}$$

Equation (2a) describes a *strongly ammonia-limited* chemical regime, in which small perturbations in the gaseous ammonia concentration will likely result in changes to $PM_{2.5}$ mass, due to the size separation of sulphate from coarse mode cations. Equation (2b) describes a *weakly ammonia-limited* chemical regime, in which the excess total ammonia subsequent to sulphate charge-balancing is still less than that required to charge balance the remaining ions of the system. The advantage of this two-level definition of ammonia-limitation is that it captures the potential impact of ammonia on fine mode particle growth due to the presence of sulphate in the smaller particle sizes. Chemical regimes for which for which (2b) is false are *ammonia-saturated*; ammonia emissions reductions would thus be less effective in reducing $PM_{2.5}$ mass for these environments.

Comprehensive Eulerian regional models are useful tools for studying the potential impacts of ammonia emissions on atmospheric particle formation and deposition to sensitive

ecosystems. The first generation of these models were designed to predict the gas-phase concentrations of acidifying gases, ozone,, other reactive gases, and wet and dry deposition of atmospheric acidic species (e.g., Chang et al., 1987; Venkatram and Karamchandani, 1988). Later work extended these models to include size-distributed PM (Binkowski and Shankar, 1995). Further developments within the last decade included the introduction of more detailed inorganic and organic particulate chemistry, and the introduction of size-resolved and speciated PM (e.g., Binkowski and Roselle, 2003; Gong et al., 2006). More recently, these models have begun to be used to investigate the role of ammonia and other nitrogen compounds in atmospheric chemistry and deposition (Mathur and Dennis, 2003; Ying and Kleeman, 2006; Phillips et al., 2006; Luo et al., 2007; Quan and Zhang, 2008; Wang et al., 2008). Environmental impacts have been assessed through the calculation of exceedances of acid-deposition critical loads (defined below) in order to estimate the impact of deposition on sensitive ecosystems (Fowler et al., 1998; Dentener et al., 2006; Spranger et al., 2008; Fenn et al., 2008; Moran et al., 2008).

Past research has suggested that ammonia emissions controls may be one means of reducing the levels of ambient PM in the atmosphere, with some caveats. Using a box model, Ansari and Pandis (1998) showed that reductions in ammonia emissions were the most effective means of reducing total PM, with the caveat that the remaining particulate mass became more acidic. West et al. (1999) used ambient air data from Eastern US monitoring sites as inputs for box modelling; they concluded that SO_2 emission controls might have to be accompanied by NO_x and NH_3 emissions controls to ensure that the former would not result in an increase in PM mass due to an increase in particulate nitrate Pinder et al. (2007) calculated the relative costs of ammonia emissions reductions versus other strategies in conjunction with regional modelling, and suggested that these reductions would be particularly cost effective and effective in the winter. Pinder et al. (2008) noted significant sensitivity of PM to NH_3 emission magnitude near NH_3 emission sources in the midwestern USA, with significant nitrogen deposition near those sources in the winter.

Of the few modelling studies that have investigated the impact of NH_3 emissions reductions on ambient PM levels in North America, the focus has been on the Eastern USA for short periods of time (Pinder et al., 2007; Tsimpidi et al., 2007), with considering seasonal and annual scenarios for the Eastern USA. (Pinder et al., 2008). In this paper, we describe the application of a comprehensive regional air-quality model for the entire North American continent, to predict the likely effects of reductions in North American emissions of agricultural ammonia on the mass and composition of atmospheric PM, and on the amount of acid deposition to sensitive ecosystems. Three one-year simulations, a 2002 base case and two hypothetical NH_3 emission scenarios, have been run and analyzed. The next section describes the study methodology. Section 3 summarizes a performance evaluation for the 2002 base case, and Sect. 4 and 5 analyze the results of the two emission scenarios. Conclusions and recommendations for further study are provided in Sect. 6.

2 Methodology

2.1 Modelling system description

AURAMS (A Unified Regional Air-quality Modelling System) consists of three main components: (a) a prognostic meteorological model, GEM (Global Environmental Multiscale model: Côté et al., 1998); (b) an emissions processing system, SMOKE (Sparse Matrix Operator Kernel Emissions: Houyoux et al., 2000; CEP, 2003); and (c) an off-line regional chemical transport model, the AURAMS Chemical Transport Model (CTM: Gong et al., 2006).

The GEM meteorological model is an integrated weather forecasting and data assimilation system that was designed to meet Canada's operational needs for both short- and medium-range weather forecasts. For the 2002 simulation, GEM version 3.2.0 with physics version 4.2 was run on the variable-resolution global horizontal grid centred on North America.

Files of gridded hourly emission fields (including ammonia) for input by the AURAMS CTM were prepared using version 2.2 of the SMOKE emissions processing system for four major emissions streams: on-road mobile sources; area and offroad-mobile sources, minor point sources; and major point sources. Emitted (i.e., "primary") PM from these sources is speciated within the AURAMS CTM based on composite speciation profiles for each emissions stream, but ammonium is assumed to be emitted as primary PM.

The multi-pollutant, regional AURAMS CTM was developed as a tool to study the formation of ozone, PM, and acid deposition in a single "unified" framework. The PM size distribution in this study was represented using 12 size bins ranging from 0.01 to 41 μm in Stokes diameter and nine chemical components: sulphate (p-SO_4); nitrate (p-NO_3); ammonium (p-NH_4); elemental carbon (EC); primary organic matter (POM); secondary organic matter (SOM); crustal material (CM); sea salt; and particle-bound water. PM is assumed to be internally mixed in each size bin. Process representations in version 1.3.1b of the AURAMS CTM include emissions from surface and from elevated sources, horizontal and vertical advection, vertical diffusion, gas-phase, aqueous-phase, and inorganic heterogeneous chemistry, secondary organic particle formation, dry and wet deposition, and particle nucleation, condensation, coagulation, sedimentation, and activation (Gong et al., 2006). Up to 157 model species (gases and speciated particle size bins) may be selected as model output, although summary measures such as $PM_{2.5}$ bulk mass are compared to observations here.

AURAMS inorganic particle components are reported as the mass of sulphate, nitrate, and ammonium within each particle bin size, but within the model, the inorganic heterogeneous chemistry module (Makar et al., 2003) performs equilibrium calculations to determine the relative amounts of mass of ammonium sulphate ($(NH_4)_2SO_4(s)$), ammonium bisulphate ($NH_4HSO_4(s)$), letovicite ($(NH_4)_3H(SO_4)_2(s)$), ammonium nitrate (NH_4NO_3 (s)), and the ammonium ($NH_4^+(aq)$), sulphate ($SO_4^{2-}(aq)$), bisulphate ($HSO_4^-(aq)$), and nitrate ions ($NO_3^-(aq)$). The reported sulphate mass (p-SO_4) is thus the sum of sulphate mass from all particle components containing sulphate, with similar sums for the nitrate and ammonium mass.

The representation of dry deposition of ammonia gas within AURAMS follows Zhang et al. (2002); deposition is parameterized as a weighted combination of the deposition properties of ozone and SO_2. Dry deposition of p-NH_4 is a function of particle size (Zhang et al., 2001). It should be noted that AURAMS does not include the possible "co-deposition" of $SO_2(g)$ and $NH_3(g)$. Some researchers have found evidence of enhanced deposition of both gases when both are present at the same site (e.g., Neirynck et al., 2005; Van Hove et al., 1989; Adema et al., 1986). Others have found no effect (Erisman et al., 1994a, b), and Sutton et al. (1994) found enhanced emissions of ammonia gas from natural surfaces when ambient NH_3 is present. More observational work on co-deposition is needed before parameterizations for this process may be reliably included in air-quality models.

The time-invariant, vertically-varying chemical lateral boundary conditions used in AURAMS CTM are taken from a variety of sources. Latitudinally-dependent O_3 boundary conditions were taken from a monthly-varying climatology (Logan, 1998). CO boundary conditions were derived from vertical profiles in Wang et al. (1999), with a simple latitudinal dependence of concentration peaking at 45° N, in rough accord with satellite observations. Speciated particulate boundary conditions (including p-NH_4) were based on data collected at an elevated site on Whistler Mountain on the Canadian west coast (MacDonald et al, 2006), with a similar simple latitude dependence assumed as for CO. Seasonally-varying profiles of the concentrations of other reactive gases (including NH_3) were taken taken from a set of "clean" chemical boundary conditions from simulations of the ADOM regional acid-deposition model (Scire et al., 1986; Fung et al., 1991).

2.2 Model domain, grid discretization, and simulation period

The GEM horizontal grid consisted of 353×415 grid points on a rotated latitude-longitude map projection with grid spacing of approximately 24 km (0.22°) on the 270×353 uniform regional "core" grid. In the vertical 28 hybrid-coordinate levels reached from the Earth's surface to 10 hPa, with layer
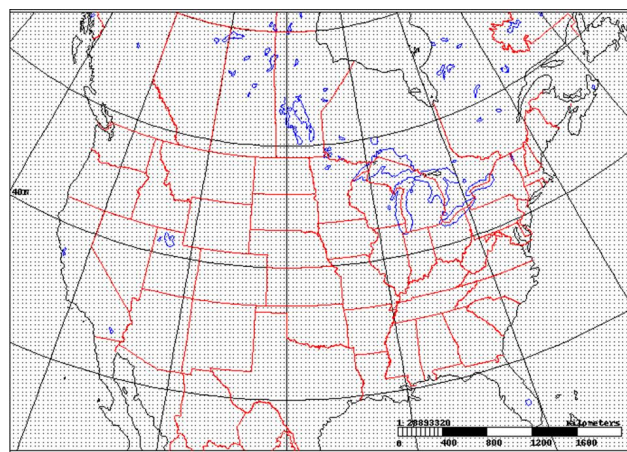

Fig. 1. AURAMS CTM North American 150×106 42-km domain.

thickness increasing monotonically with height. A time step of 450 s was used.

The uniform horizontal grid used for the AURAMS CTM was 150×106 in size and spanned the North American continent on a secant polar-stereographic projection true at 60° N, with a horizontal grid spacing of 42 km (see Fig. 1). Twenty-eight terrain-following vertical levels stretched telescopically from the Earth's surface to 29 km, with the first three levels at 0, 13.9, and 55 m AGL. An advective time step of 900 s was used, and AURAMS-predicted fields were output hourly. Both GEM and the AURAMS CTM were run for the 13-month period from 1 December 2001 to 31 December 2002, where the first month was treated as a spin-up period for the AURAMS CTM. GEM was run from analyzed fields for 396 overlapping 30-hour segments starting 24 h apart, where the first six hours of each segment were treated as a "spin-up" period and were discarded. The remaining 24 h of consecutive simulations were then "stitched" together to create a complete set of meteorological fields with a 900 s timestep for input to the AURAMS CTM. The CTM itself was run in three segments, with a one-month spin-up for each segment, allowing an entire year's simulation to be run in parallel on multiple processors in order to reduce simulation "wall-clock" time.

2.3 Description of emissions scenarios

The hourly gridded anthropogenic emissions files for all of the emitted species required by AURAMS were generated using SMOKE v2.2 (http://www.smoke-model.org/index.cfm) based on the 2002 Canadian (obtained from Environment Canada), 2002 US (obtained from US EPA), and 1999 Mexican (obtained from US EPA) national criteria-air-contaminant inventories. Biogenic emissions are calculated on-line in the AURAMS CTM using BEIS version 3.09 (Biogenic Emissions Inventory System;: CEP, 2003, and http://www.epa.gov/AMD/biogen.html). Biogenic emissions
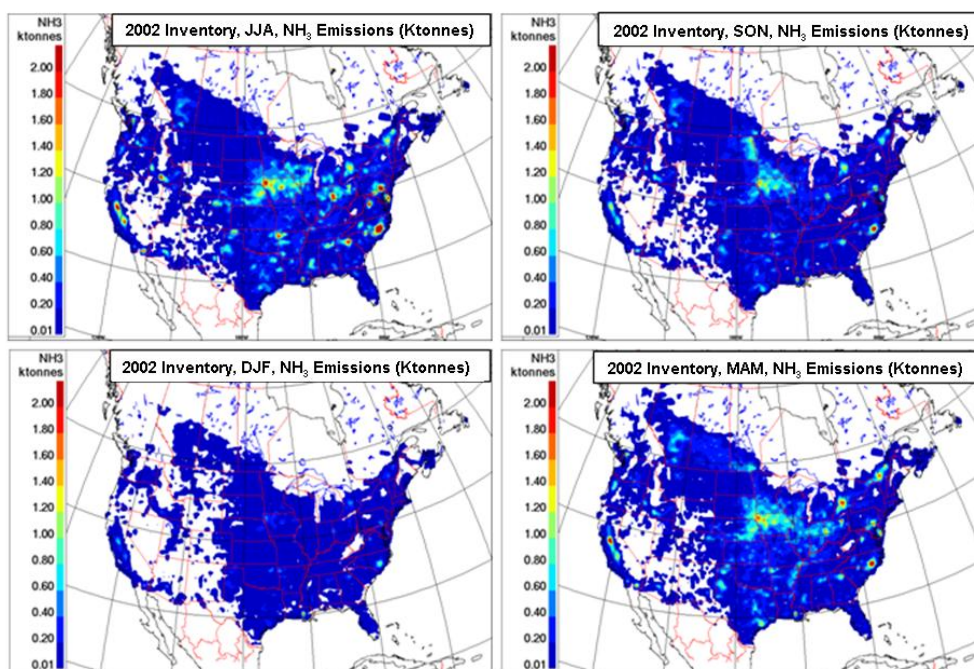
Fig. 2. Ammonia emissions (kilotonnes) in each season. upper left: June-July-August; upper right: September-October-November; lower left: December-January-February; lower right: March-April-May.

of ammonia are known to be very small compared to anthropogenic sources (Denman et al., 2007), and are not included in the current work. The following three 2002 annual emissions scenarios were considered:

(1) *Base Case*: Canadian 2002 ammonia emissions from the default national inventory were replaced with those resulting from a more detailed inventory constructed as part of the National Agri-Environmental Standards Initiative (NAESI), a multi-year study which included the collection of Canada-specific emission factors and activity levels (Ayres et al., 2009; Bittman et al., 2008). The scenario using these combined emissions inventories will be referred to hereafter as the "Base Case". The spatial distribution of ammonia gas emissions for the base case on a seasonal basis are shown in Fig. 2. The 2002 Canadian and US agricultural source emissions are presented by source type and month in Tables 1 and 2, respectively.

(2) *30% agricultural NH$_3$ emissions reduction, Canada and US:* The base case's agricultural emissions of NH$_3$ (including emissions from animal husbandry and from fertilizer application) were reduced by a factor of 30% at all times and locations in both countries.

(3) *50% Canadian beef cattle NH$_3$ emissions reduction:* A 50% reduction in Canadian emissions from this single sub-sector was implemented in order to test model sensitivity to sub-sector-specific inventory uncertainty estimates of a factor of two.

2.4 Metrics and diagnostic fields for scenario analysis

The key species of interest in this study are the model-predicted values of gaseous ammonia, SO$_2$, and nitric acid, as well as the total PM$_{2.5}$ mass and PM$_{2.5}$ inorganic composition. Differences between base case and scenario (i.e., {base case value – scenario value}) for these species show the impacts of the change in emissions of NH$_3$, with *positive* values indicating *decreases* in the mass or concentration arising from the reduction in NH$_3$ emissions.

In order to explain the chemistry associated with the base case, and the chemical reasons for the changes associated with the emissions-reduction scenarios, four chemical metrics based on the ambient air concentrations of several species have been employed. The metrics and their interpretation are given in Table 3.

A number of diagnostic deposition fields were also calculated to help quantify the impacts of changes in NH$_3$ emissions on atmospheric chemistry and deposition. The derived deposition fields include the total amount of sulphur deposited per season (sum of wet deposition and dry deposition of all species containing sulphur), the total amount of nitrate deposited, the total amount of ammonium deposited, and the total amount of nitrogen deposited. Subcomponents of these diagnostics will also be occasionally referenced (e.g., the amount of wet-deposited sulphate + SO$_2$ as a fraction of the total sulphur deposition).

Table 1. 2002 Canadian emissions of agricultural ammonia by source type (Ayres et al., 2009; Bittman et al., 2008), NAESI 2002 inventory (metric tonnes).

Source	Jan	Feb	Mar	Apr	May	Jun	Jul	Aug	Sep	Oct	Nov	Dec
Bulls	1.3	1.3	1.4	2.2	6.5	4.2	4.2	5.4	6.1	4.1	1.5	1.3
Calves under 1 year	350.7	347.6	364.5	709.5	2440.4	1477.2	1442.4	1808.2	2076.6	1347.2	407.3	350.7
Cows	1482.5	1469.4	1998.7	3738.0	6724.4	3857.9	4259.7	4186.0	5588.0	4123.8	2164.4	1482.5
Heifers	113.0	112.0	148.2	263.9	446.6	255.8	285.4	279.0	371.7	278.3	158.2	113.0
Broiler	301.8	316.7	325.6	1094.8	1456.1	600.2	791.7	828.4	1064.5	992.8	291.7	291.2
Lay Hen	369.1	366.7	380.0	1103.0	1460.5	670.6	789.6	894.5	1090.2	1106.9	408.2	360.1
Turkey	121.3	126.6	134.7	447.3	563.9	264.7	346.5	433.2	467.8	424.5	130.8	108.5
Boars	6.7	6.7	7.7	16.6	29.6	16.3	16.4	16.9	21.5	21.3	9.7	6.4
Growing pigs	2681.6	2657.8	2905.3	4928.1	9442.0	5492.6	5489.3	5406.1	7023.3	6899.5	3574.6	2776.0
Nursery pigs	521.6	517.0	584.0	1155.9	2825.9	1424.5	1429.8	1345.1	1913.5	1714.1	775.9	543.0
Sows	220.1	218.2	253.0	560.2	1059.9	543.2	558.5	574.7	783.1	788.2	348.7	226.6
Cows	1503.7	1490.4	1565.3	3678.9	14 975.7	12 151.3	10 457.8	12 162.7	15 740.4	11 334.6	1635.8	1503.7
Heifers	364.3	361.1	373.4	628.0	2038.0	1718.2	1561.9	1801.4	2203.1	1689.7	382.7	364.3
Bulls	244.5	242.3	250.0	392.4	1185.9	1017.8	946.7	1086.7	1320.4	1031.4	253.6	244.5
Calves under 1 year	480.0	475.7	513.3	1440.0	6266.3	5011.9	4259.2	4783.2	6360.3	4543.1	533.0	480.0
Steers	1054.6	1045.2	1074.3	1846.2	5006.7	4069.6	4066.6	4487.2	5252.7	4104.8	1132.4	1054.6
Fertilizer												
Alfalfa	0.0	0.0	50.5	340.7	1023.2	178.4	96.5	140.1	59.3	63.5	24.3	0.0
Barley	0.0	0.0	42.5	1096.0	13 047.0	681.3	54.6	0.0	58.8	1451.6	41.0	0.0
Beans	0.0	0.0	2.7	22.2	58.4	15.6	3.5	0.0	0.4	0.4	0.0	0.0
Buckwheat	0.0	0.0	0.3	3.0	14.3	2.1	0.4	0.0	0.1	0.9	0.0	0.0
Canary Seed	0.0	0.0	0.0	21.7	348.8	12.7	0.0	0.0	1.2	41.5	1.2	0.0
Canola	0.0	0.0	6.2	821.4	12 672.9	485.4	7.9	0.0	58.6	1496.3	42.2	0.0
Carrot	0.0	0.0	2.0	16.9	44.7	11.9	2.6	0.0	0.3	0.3	0.0	0.0
Chickpea	0.0	0.0	0.0	24.2	394.2	14.1	0.0	0.0	0.5	47.0	1.3	0.0
Corn (grain)	0.0	0.0	389.2	3214.0	8412.2	2258.5	500.3	0.0	58.2	46.3	1.3	0.0
Corn with ensilage	0.0	0.0	56.0	470.5	1339.1	329.7	72.0	0.0	8.9	22.0	0.6	0.0
Dry field crop peas	0.0	0.0	0.1	80.3	1297.5	47.0	0.1	0.0	5.5	154.5	4.4	0.0
Flaxseed	0.0	0.0	0.1	102.7	1662.0	60.0	0.1	0.0	7.4	198.0	5.6	0.0
Forage	0.0	0.0	4.4	559.3	891.2	134.1	8.4	141.0	59.0	87.5	61.5	0.0
Green Peas	0.0	0.0	2.9	23.7	62.3	16.6	3.7	0.0	0.4	0.4	0.0	0.0
Pasture cultivated or sown	0.0	0.0	30.3	1101.9	1973.8	308.1	57.9	266.3	121.5	177.1	115.2	0.0
Lentil	0.0	0.0	0.0	33.7	548.8	19.7	0.0	0.0	1.7	65.5	1.8	0.0
Mustard Seed	0.0	0.0	0.0	46.6	758.8	27.2	0.0	0.0	2.5	90.5	2.6	0.0
Mixed Grains	0.0	0.0	14.8	144.2	679.2	98.7	19.0	0.0	3.8	44.6	1.3	0.0
Oats	0.0	0.0	19.9	473.3	5850.2	402.4	52.4	7.1	26.7	653.7	18.4	0.0
Other Dry Beans	0.0	0.0	2.7	29.8	181.2	20.1	3.5	0.0	1.0	15.0	0.4	0.0
Other Vegetables	0.0	0.0	7.5	62.4	165.4	43.8	9.7	0.0	1.1	1.2	0.0	0.0
Other Hay and Fodder	0.0	0.0	201.0	1179.7	3804.1	670.1	383.8	530.7	220.3	225.2	76.9	0.0
Potatoes	0.0	0.0	36.6	325.0	1165.8	225.6	47.0	0.0	6.9	49.1	1.4	0.0
Fall Rye	0.0	0.0	2.6	25.6	125.5	17.9	3.4	0.0	0.6	8.6	0.2	0.0
Spring Rye	0.0	0.0	0.0	1.0	15.7	0.6	0.0	0.0	0.0	1.9	0.1	0.0
Soybeans	0.0	0.0	45.4	373.4	962.0	262.5	58.3	0.0	6.7	3.2	0.1	1.0
Sugar Beets	0.0	0.0	0.0	1.6	26.4	0.9	0.0	0.0	0.0	3.2	0.1	0.0
Sunflowers	0.0	0.0	0.1	20.1	322.0	11.8	0.1	0.0	1.5	38.3	1.1	0.0
Sweet Corn	0.0	0.0	7.3	60.9	163.1	42.8	9.4	0.0	1.1	1.4	0.0	0.0
Tobacco	0.0	0.0	1.9	15.5	38.9	10.9	2.4	0.0	0.3	0.0	0.0	0.0
Tomato	0.0	0.0	2.6	21.0	53.2	14.8	3.3	0.0	0.4	0.1	0.0	0.0
Triticale	0.0	0.0	0.0	6.2	100.3	3.6	0.0	0.0	0.2	12.0	0.3	0.0
Natural Pastures	0.0	0.0	10.0	1100.6	1767.3	266.6	19.0	207.4	106.2	172.6	120.7	0.0
White beans	0.0	0.0	2.7	31.8	208.4	21.3	3.5	0.0	1.1	18.1	0.5	0.0
Durham Wheat	0.0	0.0	0.0	315.4	5130.2	184.0	0.0	0.0	10.9	611.8	17.3	0.0
Spring Wheat	0.0	0.0	21.2	1418.5	20 987.8	932.5	48.5	5.6	88.8	2454.5	69.2	0.0
Winter Wheat	0.0	0.0	59.8	519.3	1710.3	361.8	76.8	0.0	8.7	57.0	1.6	0.0

Table 2. 2002 USA agricultural emissions of ammonia by source type, metric tonnes (US EPA).

Source	Jan	Feb	Mar	Apr	May	Jun	Jul	Aug	Sep	Oct	Nov	Dec
Field burning, all crops	347.5	599.2	559.1	114.7	256.2	191.5	28.0	34.8	36.4	60.7	120.2	155.1
Field burning, unspec. Crop	8.8	8.8	12.2	12.2	12.2	14.2	14.2	14.2	15.6	15.6	15.6	8.8
Field burning, Alfalfa headfire	5.1	5.1	7.1	7.1	7.1	8.2	8.2	8.2	9.0	9.0	9.0	5.1
Field burning, Alfalfa backfire	0.2	0.2	0.2	0.2	0.2	0.3	0.3	0.3	0.3	0.3	0.3	0.2
Field burning,Barley	0.1	0.1	0.1	0.1	0.1	0.2	0.2	0.2	0.2	0.2	0.2	0.1
Field burning, Red Bean	7.4	7.4	10.2	10.2	10.2	11.8	11.8	11.8	13.0	13.0	13.0	7.4
Field burning, corn	27.0	27.0	37.2	37.2	37.2	43.2	43.2	43.2	47.4	47.4	47.4	27.0
Field burning, Grasses	628.1	628.1	866.3	866.3	866.3	1007.1	1007.1	1007.1	1104.6	1104.6	1104.6	628.1
Field burning, wild hay headfire	27.8	27.8	38.3	38.3	38.3	44.5	44.5	44.5	48.8	48.8	48.8	27.8
Field burning, wild hay backfire	2.0	2.0	2.8	2.8	2.8	3.2	3.2	3.2	3.5	3.5	3.5	2.0
Field burning, Oats headfire	0.2	0.2	0.3	0.3	0.3	0.3	0.3	0.3	0.4	0.4	0.4	0.2
Field burning, Oats backfire	0.0	0.0	0.0	0.0	0.0	0.1	0.1	0.1	0.1	0.1	0.1	0.0
Field burning, Pea Headfire	0.0	0.0	0.1	0.1	0.1	0.1	0.1	0.1	0.1	0.1	0.1	0.0
Field burning, Rice	8.0	8.0	11.0	11.0	11.0	12.8	12.8	12.8	14.0	14.0	14.0	8.0
Field burning, Sorghum	1.6	1.6	2.2	2.2	2.2	2.6	2.6	2.6	2.8	2.8	2.8	1.6
Field burning, Sugar Cane	100.1	100.1	138.1	138.1	138.1	160.5	160.5	160.5	176.1	176.1	176.1	100.1
Field burning, Wheat Headfire	246.8	246.8	340.4	340.4	340.4	395.7	395.7	395.7	434.0	434.0	434.0	246.8
Field burning, Wheat Backfire	17.1	17.1	23.6	23.6	23.6	27.4	27.4	27.4	30.0	30.0	30.0	17.1
Agricultural propaning, all crop types	0.2	0.2	0.3	0.3	0.3	0.4	0.4	0.4	0.4	0.4	0.4	0.2
Agricultural stack burning, all crop types	0.0	0.0	0.0	0.0	0.0	0.0	0.0	0.0	0.0	0.0	0.0	0.0
Fertilizer: Anhydrous Ammonia	2274.3	4427.9	22 246.0	25 535.0	22 590.2	22 185.7	6127.4	7961.7	14 472.3	7347.9	6191.3	4076.7
Fertilizer: Aqueous Ammonia	38.2	74.4	374.0	429.3	379.8	373.0	103.0	133.8	243.3	123.5	104.1	68.5
Fertilizer: Nitrogen solutions	4040.7	7867.0	39 524.3	45 367.8	40 135.7	39 417.1	10 886.5	14 145.5	25 712.8	13 055.0	11 000.0	7243.0
Fertilizer: Urea	7325.1	14 261.7	71 651.1	82 244.5	72 759.6	71 456.9	19 735.5	25 643.6	46 613.2	23 666.6	19 941.2	13 130.3
Fertilizer: Ammonium Nitrate	213.4	415.4	2087.0	2395.6	2119.3	2081.4	574.9	746.9	1357.7	689.4	580.8	382.5
Fertilizer: Ammonium Sulfate	392.2	763.6	3836.3	4403.5	3895.6	3825.9	1056.7	1373.0	2495.7	1267.1	1067.7	703.0
Fertilizer: Ammonium Thiosulfate	14.9	29.1	146.0	167.6	148.3	145.6	40.2	52.3	95.0	48.2	40.6	26.8
Fertilizer: Other Straight Nitrogen	0.0	0.0	0.0	0.0	0.0	0.0	0.0	0.0	0.0	0.0	0.0	0.0
Fertilizer: Ammonium Phosphates	0.0	0.0	0.0	0.0	0.0	0.0	0.0	0.0	0.0	0.0	0.0	0.0
Fertilizer: NPK multigrade fertilizer	657.7	1280.6	6433.7	7384.9	6533.2	6416.3	1772.1	2302.6	4185.5	2125.1	1790.6	1179.0
Fertilizer: Calcium ammonium nitrate	16.0	31.2	156.7	179.9	159.2	156.3	43.2	56.1	102.0	51.8	43.6	28.7
Fertilizer: Potassium nitrate	3.2	6.3	31.7	36.4	32.2	31.6	8.7	11.3	20.6	10.5	8.8	5.8
Fertilizer: Diammonium Phosphate	536.4	1044.6	5247.1	6022.8	5328.2	5232.8	1445.2	1877.9	3413.5	1733.1	1460.3	961.5
Fertilizer: Monoammonium Phosphate	183.0	356.4	1790.4	2055.0	1818.0	1785.5	493.1	640.8	1164.7	591.4	498.3	328.1
Fertilizer: Liquid Ammonium Polyphosphate	119.3	232.2	1166.6	1339.1	1184.7	1163.4	321.3	417.5	758.9	385.3	324.7	213.8
Fertilizer: Miscellaneous	388.4	756.1	3798.9	4360.5	3857.7	3788.6	1046.4	1359.6	2471.4	1254.8	1057.3	696.2
Agriculture: Livestock	3077.3	5093.5	4365.9	8117.8	7443.2	10 459.9	14 681.7	9656.4	7329.5	5859.0	5859.0	1349.2
Beef Cattle: feedlot, confinement	4127.5	7495.3	6279.8	12 547.0	11 293.5	16 332.6	23 384.7	14 990.5	11 230.2	8774.0	8774.0	1240.8
Beef Cattle: Feedlot, manure handling and storage	1.6	2.9	2.5	4.9	4.4	6.4	9.2	5.9	4.4	3.4	3.4	0.5
Beef Cattle: feedlot, land application of manure	3403.6	6180.8	5178.5	10 346.6	9313.0	13 468.3	19 283.7	12 361.6	9260.8	7235.3	7235.3	1023.2
Beef Cattle: Other	21.6	39.2	32.8	65.6	59.0	85.4	122.2	78.4	58.7	45.9	45.9	6.5
Beef Cattle: pasture, confinement	7972.8	14 478.2	12 130.4	24 236.3	21 815.1	31 548.7	45 171.0	28 956.4	21 692.8	16 948.3	16 948.3	2396.7
Poultry: dry manure management, confinement	3190.1	5793.1	4853.7	9697.6	8728.8	12 623.5	18 074.1	11 586.2	8679.9	6781.5	6781.5	959.0
Poultry: dry manure management, land application of manure	73.8	134.0	112.3	224.3	201.9	292.0	418.1	268.0	200.8	156.9	156.9	22.2
Poultry: wet manure management, confinement	177.5	322.4	270.1	539.7	485.8	702.6	1005.9	644.8	483.1	377.4	377.4	53.4
Poultry: wet manure management, manure handling and storage	481.7	874.8	732.9	1464.4	1318.1	1906.2	2729.3	1749.6	1310.7	1024.0	1024.0	144.8
Poultry: wet manure management, land application of manure	81.0	147.1	123.2	246.2	221.6	320.5	458.9	294.1	220.4	172.2	172.2	24.3
Poultry: broilers, confinement	4249.8	7717.4	6465.9	12 918.8	11 628.2	16 816.5	24 077.6	15 434.7	11 563.0	9034.0	9034.0	1277.5
Poultry: broilers, manure handling and storage	771.5	1401.0	1173.8	2345.2	2110.9	3052.8	4371.0	2802.0	2099.1	1640.0	1640.0	231.9
Poultry: broilers, land application of manure	3473.2	6307.1	5284.3	10 558.0	9503.3	13 743.5	19 677.8	12 614.2	9450.0	7383.2	7383.2	1044.1
Poultry: turkeys, confinement	728.3	728.3	1607.3	1732.9	1883.5	3842.4	4344.7	4344.7	2034.2	1883.5	1079.9	879.0
Poultry: turkeys, manure handling and storage	131.0	131.0	289.1	311.7	338.8	691.2	781.5	781.5	365.9	338.8	194.3	158.1
Poultry: turkeys, land application of manure	655.5	655.5	1446.7	1559.7	1695.4	3458.5	3910.6	3910.6	1831.0	1695.4	972.0	791.2
Dairy cattle composite	735.4	735.4	1623.1	1749.9	1902.0	3880.1	4387.3	4387.3	2054.2	1902.0	1090.5	887.6
Dairy cattle flush dairy, confinement	447.4	447.4	987.4	1064.6	1157.1	2360.5	2669.1	2669.1	1249.7	1157.1	663.4	540.0
Dairy cattle flush dairy, manure handling and storage	1247.6	1247.6	2753.4	2968.5	3226.6	6582.3	7442.8	7442.8	3484.8	3226.6	1849.9	1505.8
Dairy cattle flush dairy, land application of manure	112.6	112.6	248.6	268.0	291.3	594.3	672.0	672.0	314.6	291.3	167.0	136.0
Cattle and calves: milk cows	380.6	691.2	579.1	1157.0	1041.4	1506.1	2156.4	1382.3	1035.6	809.1	809.1	114.4
Cattle and calves: beef cows	1003.5	1822.3	1526.8	3050.4	2745.7	3970.8	5685.3	3644.5	2730.3	2133.2	2133.2	301.7
Cattle and calves: heifer and heifer calves	802.0	1456.4	1220.2	2438.0	2194.5	3173.6	4543.9	2912.8	2182.2	1704.9	1704.9	241.1
Cattle and calves: steers, bulls and steer/bull calves	922.3	1674.8	1403.2	2803.6	2523.5	3649.4	5225.2	3349.6	2509.3	1960.5	1960.5	277.2
Dairy cattle scrape dairy, confinement	1084.3	1084.3	2392.9	2579.9	2804.2	5720.6	6468.4	6468.4	3028.5	2804.2	1607.7	1308.6
Dairy cattle scrape dairy, manure handling and storage	1753.2	1753.2	3869.1	4171.3	4534.1	9249.5	10 458.6	10 458.6	4896.6	4534.1	2599.5	2115.9
Dairy cattle scrape dairy, land application of manure	2064.1	2064.1	4555.3	4911.2	5338.3	10 890.1	12 313.6	12 313.6	5765.3	5338.3	3060.6	2491.2
Dairy cattle, deep pit dairy, confinement	127.4	127.4	281.1	303.0	329.4	672.0	759.8	759.8	355.7	329.4	188.8	153.7
Dairy cattle, deep pit dairy, manure handling and storage	5.9	5.9	13.1	14.1	15.4	31.3	35.4	35.4	16.6	15.4	8.8	7.2
Dairy cattle, deep pit dairy, land application of manure	72.4	72.4	159.8	172.3	187.3	382.1	432.1	432.1	202.3	187.3	107.4	87.4
Dairy cattle drylot/pasture dairy, confinement	1011.7	1011.7	2232.8	2407.2	2616.5	5337.7	6035.5	6035.5	2825.9	2616.5	1500.1	1221.0
Dairy cattle drylot/pasture dairy, manure handling and storage	21.0	21.0	46.4	50.0	54.4	110.9	125.4	125.4	58.7	54.4	31.2	25.4
Dairy cattle drylot/pasture dairy, land application of manure	1261.9	1261.9	2784.8	3002.4	3263.5	6657.4	7527.7	7527.7	3524.5	3263.5	1871.0	1522.9
Swine production composite	1943.5	3529.3	2957.0	5317.7		7690.5	11 011.1	7058.5	5287.9	4131.4	4131.4	584.2
Poultry waste emissions, other	1229.7	2233.0	1870.9	3738.0	3364.6	4865.8	6966.8	4466.0	3345.7	2614.0	2614.0	369.7
Poultry waste emissions, pullet and chicks <13 weeks	21.2	38.5	32.2	64.4	57.9	83.8	120.0	76.9	57.6	45.0	45.0	6.4
Poultry waste emissions, pullet and chicks >=13 weeks	15.5	28.1	23.6	47.1	42.4	61.3	87.8	56.3	42.1	32.9	32.9	4.7
Poultry waste emissions, Layers	101.2	183.8	154.0	307.7	276.9	400.5	573.5	367.6	275.4	215.2	215.2	30.4
Poultry waste emissions, Broilers	48.6	88.3	74.0	147.8	133.1	192.4	275.5	176.6	132.3	103.4	103.4	14.6
Poultry waste emissions, Ducks	85.4	155.1	129.9	259.6	233.6	337.9	483.8	310.1	232.3	181.5	181.5	25.7
Poultry waste emissions, Geese	4.9	8.9	7.5	14.9	13.4	19.4	27.8	17.8	13.4	10.4	10.4	1.5
Poultry waste emissions, Turkeys	340.9	619.1	518.7	1036.3	932.8	1349.0	1931.5	1238.2	927.6	724.7	724.7	102.5
Horses and Ponies waste emissions	1345.5	2443.3	2047.1	4090.1	3681.5	5324.1	7622.9	4886.6	3660.8	2860.2	2860.2	404.5
Swine production, lagoons, confinement	1901.4	3452.8	2892.9	5779.9	5202.5	7523.8	10 772.5	6905.6	5173.4	4041.9	4041.9	571.6
Swine production, lagoons, manure handling and storage	3734.2	6781.1	5681.5	11 351.5	10 217.5	14 776.5	21 156.7	13 562.3	10 160.3	7938.1	7938.1	1122.6
Swine production, lagoons, land application of manure	308.7	560.6	469.7	938.4	844.6	1221.5	1748.9	1121.1	839.9	656.2	656.2	92.8
Sheep and lambs waste emissions	553.8	1005.7	842.6	1683.5	1515.3	2191.4	3137.6	2011.4	1506.8	1177.3	1177.3	166.5
Goats waste emissions, other	481.7	874.7	732.8	1464.2	1317.9	1906.0	2728.9	1749.4	1310.5	1023.9	1023.9	144.8
Goats waste emissions, Angora	0.2	0.3	0.3	0.5	0.5	0.7	1.0	0.6	0.5	0.4	0.4	0.1
Goats waste emissions, Milk	0.2	0.4	0.3	0.6	0.5	0.8	1.1	0.7	0.5	0.4	0.4	0.1
Swine production, deep-pit, confinement	2605.3	4731.2	3964.0	7919.9	7128.7	10 309.5	14 760.9	9462.3	7088.8	5538.3	5538.3	783.2
Swine production, deep-pit, land application of manure	1153.4	2094.6	1754.9	3506.3	3156.0	4564.2	6534.9	4189.1	3138.3	2451.9	2451.9	346.7
Swine production, outdoor, Confinement	20.2	36.8	30.8	61.5	55.4	80.1	114.7	73.5	55.1	43.0	43.0	6.1

Table 3. Metrics for chemical evaluation of model responses to NH_3 emission changes.

Metric	Formula	Significance
Particle Neutralization Ratio	$\dfrac{(p\text{-}NH_4)}{2(p\text{-}SO_4)+(p\text{-}NO_3)}$	Ratio of total ammonium charge to the net sulphate and nitrate charge (each particle species variable is the sum over all particle sizes). Values of 1 indicate that the particles are NH_3-saturated, so that significant NH_3 reductions may be required to reduce particulate mass. Regions with values less than unity are more NH_3- limited; smaller reductions in NH_3 may result in significant reductions in particulate mass.
Total ammonia to sulphate mole ratio	$\dfrac{(NH_3(g))+(p\text{-}NH_4)}{(p\text{-}SO_4)}$	Mole ratio of ammonia gas + particle ammonia to particle sulphate. This defines the chemical regime: values less than unity denote acidic conditions (e.g., ammonium bisulphate, sulphuric acid present in the particles); values between 1.0 and 2.0 denote intermediate acidity (ammonium bisulphate, letovicite, ammonium sulphate present), and values greater than 2 indicate less acidic particles (ammonium sulphate, ammonium nitrate may be present in the particles). Note that a decrease in the value of the ratio does not necessarily imply a significant change in the particle composition, if the initial and final values of the ratio are both high.
Gas-phase ammonia mass fraction	$\dfrac{(NH_3)}{(PM_{2.5}\text{-}NH_4)+(NH_3)}$	Relative mass of NH_3 in the gas phase to total ammonia + ammonium mass. Changes in this parameter indicate a change in the mass partitioning of ambient NH_3 in response to changes in NH_3 emissions.
$PM_{2.5}$ Ammonium + Nitrate to total $PM_{2.5}$ mass ratio	$\dfrac{(PM_{2.5}\text{-}NH_4)+(PM_{2.5}\text{-}NO_3)}{(PM_{2.5})}$	Fraction of fine particle mass that is directly ammonia-sensitive. A diagnostic of the direct impact of emissions reductions.

Another important set of diagnostic outputs calculated for the AURAMS analysis were *exceedances of annual critical loads* in Canada. The "critical load" of an ecosystem refers to its ability to buffer acidifying precipitation. The underlying concept is that an ecosystem will have the ability to absorb a certain amount of acidifying sulphur and nitrogen compounds, including NH_3 and $p\text{-}NH_4$, without damage to the ecosystem itself. If the rate of deposition of these compounds exceeds the rate at which the ecosystem can naturally absorb the compounds, however, ecosystem damage begins to occur. The maximum amount of acidifying mass that an ecosystem can absorb per unit area in a year is known as its *annual critical load*, and any additional deposited mass that exceeds that amount is known as an *annual critical load exceedance* (e.g., Jeffries et al., 1999; Hall et al., 2001; Jeffries and Ouimet, 2005; McNulty et al., 2007). Critical-load values depend on local bedrock type, soil type and thickness, and other factors.

Sulphur deposition is essentially entirely acidifying, but nitrogen has a large biological activity, and may be stored in various catchment compartments within an ecosystem (Jeffries and Ouimet, 2005). Eventually, though, an ecosystem may reach a steady state with regard to nitrogen de-

position (termed "nitrogen saturation"), after which all further nitrogen deposition is acidifying. Sulphur critical-load exceedance thus describes conditions where immediate ecosystem damage will occur, whereas sulphur + nitrogen critical-load exceedance describes conditions where ecosystem damage will once the ecosystem's ability to absorb nitrogen is overwhelmed. Critical-load exceedances for sulphur + nitrogen thus describe a worst-case scenario, in which all of the deposited nitrogen is assumed to be acidifying. At the current time, Canadian ecosystems are not nitrogen-saturated (Jeffries and Ouimet, 2005); exceedances of sulphur + nitrogen critical loads thus indicate the potential for future ecosystem damage, as opposed to current ecosystem damage.

3 Model performance evaluation for the base case

The statistics used here for evaluation of the base case for the AURAMS simulations were used previously as part of an extensive AURAMS performance evaluation against measurements for the 2002 calendar year (Moran et al., 2007, 2008). The statistical measures used for the comparison are shown

Table 4. Statistical measures of model performance. N is the number of paired observed-model values, $\overline{O}$ is the mean observed value, $\overline{M}$ is the mean model value.

Statistical Measure	Description	Formula
R	Pearson Correlation Coefficient	$R = \dfrac{N \sum\limits_{i=1}^{N}(O_i \cdot M_i) - \sum\limits_{i=1}^{N}(M_i)\sum\limits_{i=1}^{N}(O_i)}{\sqrt{N\sum\limits_{i=1}^{N}(M_i \cdot M_i) - \sum\limits_{i=1}^{N}(M_i)\cdot\sum\limits_{i=1}^{N}(M_i)}\sqrt{N\sum\limits_{i=1}^{N}(O_i \cdot O_i) - \sum\limits_{i=1}^{N}(O_i)\cdot\sum\limits_{i=1}^{N}(O_i)}}$
b	Slope of observations vs. model best-fit line	$b = \dfrac{\sum\limits_{i=1}^{N}\left[(O_i - \overline{O})(M_i - \overline{M})\right]}{\sum\limits_{i=1}^{N}\left[(O_i - \overline{O})^2\right]}$
a	Intercept of observations vs. model best-fit line	$a = \overline{M} - b \cdot \overline{O}$
MB	Mean bias	$MB = \dfrac{1}{N}\sum\limits_{i=1}^{N}(M_i - O_i)$
RMSE	Root Mean Square Error	$\text{RMSE} = \sqrt{\dfrac{1}{N}\sum\limits_{i=1}^{N}(M_i - O_i)^2}$
NMB	Normalized Mean Bias	$\text{NMB} = \dfrac{\sum\limits_{i=1}^{N}(M_i - O_i)}{\sum\limits_{i=1}^{N}O_i}\times 100$
NME	Normalized Mean Error	$\text{NME} = \dfrac{\sum\limits_{i=1}^{N}|M_i - O_i|}{\sum\limits_{i=1}^{N}O_i}\times 100$

in Table 4. Measurements from 15 different Canadian and US air-chemistry and precipitation-chemistry networks and subnetworks were used to evaluate the base-case fields.

A number of steps were followed in preparing the measurements for comparison with model predictions. For example, units reported by individual networks were adjusted as required to a common set of units (e.g., concentrations at ambient conditions to concentrations at STP). Data records from individual stations were screened for temporal completeness, and if they passed, then measurements were combined to create seasonal and annual values for the station. In locations where more than one station was located in an AURAMS CTM grid cell, the measurements were averaged. Even so, measurements from multiple air-chemistry networks are quite heterogeneous, since individual networks have different goals and objectives, choose different types of sampling locations, employ different sampling instruments, techniques, and protocols, and measure different species (e.g., Eder and Yu, 2006). For example, individual networks have very different sampling periods, ranging from hourly to weekly, and sampling intervals that vary from hourly, to 1 day in 6, to weekly. Combining measurements from different network does provide the benefits of increased sample size, spatial coverage, and spatial density, but the price paid is greater variability within the combined measurement data set.

The resulting annual statistics for ambient concentrations of the key species related to pNH$_4$ formation and removal, with the exception of NH$_3$, for which routine measurements are not available, are shown in Table 5, and those relating to wet deposition are shown in Table 6.

These comparisons to observations show that, on an annual basis, AURAMS under-predicted the 2002 base-case PM$_{2.5}$ bulk mass by 31%, the PM$_{2.5}$ inorganic species concentrations by 18% to 19%, the concentration of inorganic ions in precipitation by 11% to 33%, and the wet deposition of inorganic ions by 6% to 24% (negative normalized mean biases). The implication of the comparison is that the model estimates for the base case for the PM$_{2.5}$ components and precipitation species are likely to be lower than the ambient atmosphere, and hence the model-predicted critical-load exceedances, described below, are likely to be underestimates. The impact of the model bias on the scenarios is harder to quantify. The usual assumption that is made is that the bias will be linear, so that the scenarios will have the same normalized biases as the base case. The absence of coarse-mode cation chemistry in AURAMS may increase the sensitivity of the model in weakly ammonia-limited environments towards changes in ammonia emissions. The impacts of ammonia emission reductions on the real atmosphere are therefore expected to be similar in sign as simulated here but may vary in the absolute sense.

Table 5. Annual statistics for selected AURAMS gas- and particle-phase species. Statistical metrics are defined in Table 4.

Statistic	SO_2 (ppbv)	HNO_3 (ppbv)	$PM_{2.5}$ ($\mu g\,m^{-3}$, STP)	$PM_{2.5}$-SO_4 ($\mu g\,m^{-3}$, STP)	$PM_{2.5}$-NO_3 ($\mu g\,m^{-3}$, STP)	$PM_{2.5}$-NH_4 ($\mu g\,m^{-3}$, STP)
Networks	a, d, e, g	d, e	a, b, c, f, g, h	c, f, h	c, f, h	c, h
N	451	86	845	265	254	141
$\overline{O}$	3.32	0.53	11.33	2.77	1.28	1.53
$\overline{M}$	3.55	0.66	7.87	2.26	1.05	1.25
a	1.01	0.08	-0.74	-0.64	0.12	0.23
b	0.77	1.10	0.76	1.04	0.73	0.66
R	0.56	0.81	0.65	0.92	0.77	0.76
MB	0.23	0.13	-3.46	-0.51	-0.23	-0.29
RMSE	2.88	0.28	5.00	0.95	1.01	0.54
NMB (%)	7.0	25.2	-30.5	-18.5	-17.9	-18.7
NME (%)	51.7	38.3	36.8	27.3	43.5	27.2

Networks: a: AQS-continuous, b: AQS-filter; c: AQS-STN; d: CAPMoN, e: CASTNet, f: IMPROVE, g: NAPS-continuous, h: NAPS-filter

Table 6. Annual statistics for several AURAMS wet deposited species. Measurements were obtained from five Canadian precipitation-chemistry networks (CAPMoN, BCPCSN, NBPMN, PQMPA, REPQ) and one US network (NADP).

Statistic	SO_4^{2-} conc. in precip. (mg SO_4/L)	NO_3^- conc. in precip.(mg NO_3/L)	NH_4^+ conc. in precip. (mg NH_4/L)	SO_4^{2-} wet dep. (kg SO_4/ha/y)	NO_3^- wet dep. (kg NO_3/ha/y)	NH_4^+ wet dep. (kg NH_4/ha/y)
N	277	270	271	277	270	271
$\overline{O}$	1.08	1.11	0.31	10.1	9.39	2.39
$\overline{M}$	0.96	0.94	0.21	9.54	8.30	1.81
a	-0.03	0.202	0.021	0.449	1.46	0.11
b	0.91	0.67	0.60	0.90	0.73	0.71
R	0.81	0.61	0.76	0.84	0.71	0.78
MB	-0.12	-0.17	-0.10	-0.58	-1.09	-0.58
RMSE	0.37	0.50	0.16	3.94	4.24	1.07
NMB (%)	-11.4	-15.0	-33.1	-5.8	-11.6	-24.1
NME (%)	24.8	33.4	36.2	28.3	33.7	33.9

4 Scenario analysis

4.1 Analysis of the base case

One means of identifying strongly NH_3-limited environments is to calculate the total (ammonia + ammonium) to sulphate mole ratio (cf. Table 3). Seasonal fields of this metric for the 2002 base case are shown in Fig. 3. Yellow to red areas in this figure have a large excess of NH_3 and are not strongly NH_3-limited: significant reductions in NH_3 emissions would be required to reach strongly NH_3-limited conditions. These areas tend to correspond to areas of high NH_3 emissions (cf. Fig. 2). Green to blue regions, on the other hand, are strongly NH_3-limited, with more acidic conditions. Reductions in NH_3 emissions in these areas would have an immediate impact on ambient $PM_{2.5}$ levels, whereas reductions in other, weakly NH_3-limited regions will depend on the other ions in equation (2b). Pronounced seasonal and local variations can also be seen; summer and winter have the largest spatial extent of strongly NH_3-limited regions. These seasonal variations are due to (1) seasonal variations in the ammonia emissions (cf. Fig. 2, which shows the lowest ammonia emissions occurring in the winter, the highest in the spring, summer and fall), and (2) increased levels of sulphate production in the summer, due to higher oxidation of SO_2 to sulphate in the gas and aqueous phases. The low winter ammonia emissions helps reduce the ratio in the winter; high summer sulphate production helps reduce the ratio in the summer.

One implication of the above analysis is that the regions that may benefit from NH_3 reductions will not necessarily be the regions that have the highest NH_3 emissions. For example, the region of highest total ammonia to sulphate mole ratio in Fig. 3 is centered on the US states of Minnesota, South Dakota, Nebraska, and Iowa – this also corresponds to the region of greatest NH_3 emissions. Reductions in NH_3 in this region are unlikely to significantly impact PM concentrations, due to the locally NH_3-saturated chemistry. However,
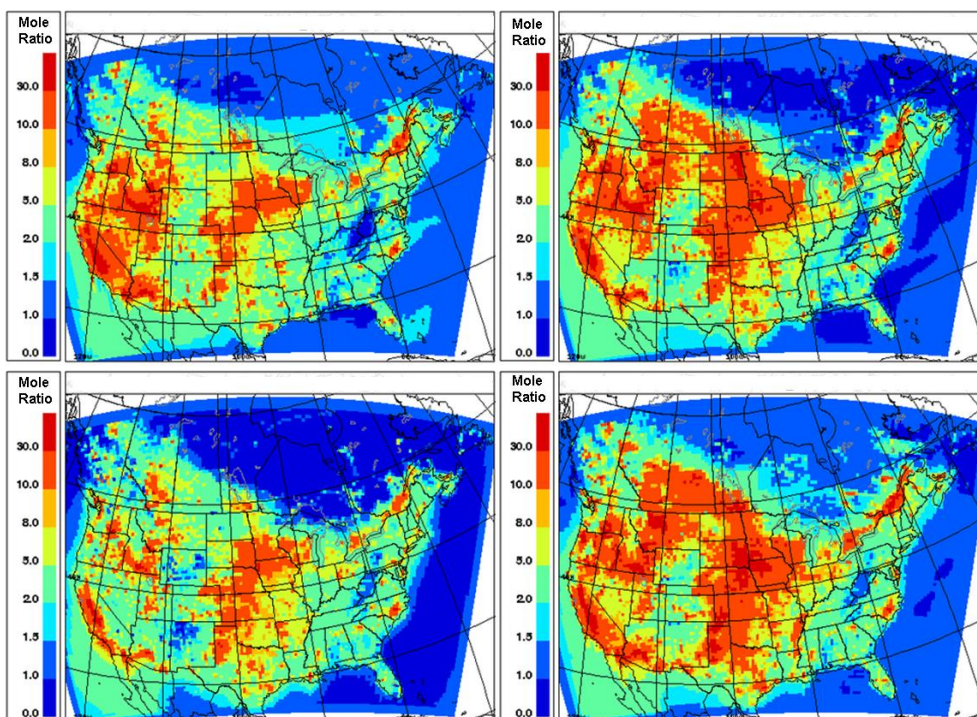
Fig. 3. Seasonal average total NH$_3$ to sulphate mole ratio for base-case simulation: summer – upper left; fall – upper right; winter – lower left; spring – lower right.

further to the east and downwind from this source region are the strongly NH$_3$-limited regions of the Great Lakes, the Ohio River Valley, and the Appalachian mountains. Depending on the extent to which NH$_3$ is transported, PM reductions may also occur in these downwind regions,. The impact of NH$_3$ reductions will therefore be a combination of local chemistry and transport from higher-emission NH$_3$-saturated regions to lower-emission strongly NH$_3$-limited regions.

4.2 Analysis of continental agricultural NH$_3$ emission reduction scenario

In this scenario, NH$_3$ emissions from agricultural sources were decreased uniformly by 30% in both Canada and the United States. In the following figures, the *difference* between base-case and scenario concentration fields will be displayed [(base case) – (scenario)], and the same difference formats will be used for the metrics. Positive values in the difference plots thus indicate *decreases* in the scenario concentrations relative to the base case; negative values indicate *increases* in the scenario concentrations relative to the base case. It is also important to note that seasonal average differences are being displayed unless noted otherwise; within each season, shorter duration events will occur with larger (and smaller) impacts than those depicted here.

4.2.1 NH$_3$ concentrations

The greatest decreases in seasonal NH$_3$ concentrations (Fig. 4) are closely matched with the locations of the main NH$_3$ emissions regions (Fig. 2). The effect of reductions in NH$_3$ emissions on NH$_3$ gas concentrations is therefore primarily *local*; most of the NH$_3$ is removed close to the source, either through deposition or gas-to-particle partitioning.

The influence of seasonal variations in the NH$_3$ emissions can also be seen in Fig. 4. Agricultural emissions in North America are highest in the spring and lowest in the winter (e.g., Gilliland et al., 2006; see also Tables 1 and 2). As a consequence, the predicted change in concentration of NH$_3$ gas in the winter is lower than in the other seasons. For example, the decrease in ammonia concentrations in the high emissions region of southern Minnesota in the summer is on the order of 2.5 ppbv, while the wintertime value in the same region is on the order of 0.5 ppbv.

4.2.2 M$_{2.5}$ concentrations

The impact of the NH$_3$ emissions reductions on average seasonal PM$_{2.5}$ mass is shown in Fig. 5. Seasonally-averaged PM$_{2.5}$ changes resulting from a 30% reduction in NH$_3$ emissions range from an increase of 0.07 to a decrease of 3.99 μg m^{-3}. The greatest overall reductions in mass occur in spring and summer, and occur in specific regions. The
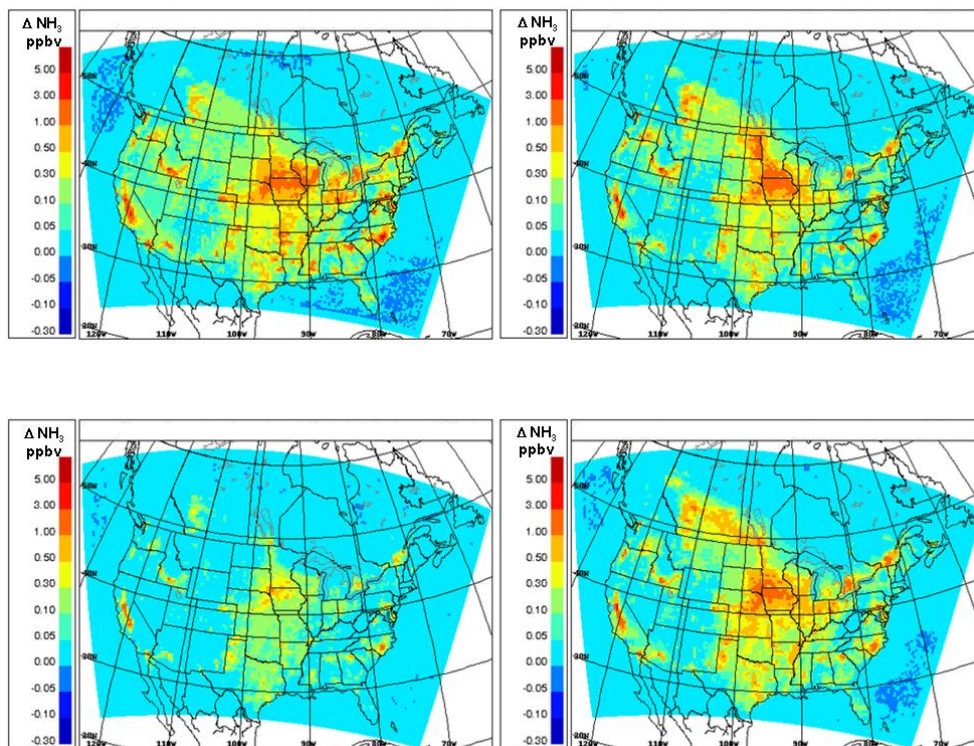
Fig. 4. Seasonal average change in NH$_3$ concentration, ppbv, associated with a 30% reduction in agricultural NH$_3$ emissions. Panels arranged as in Fig. 2.

largest of these regions is centered over the Ohio River valley and southern Ontario; most of the eastern US and southern Ontario and Quebec experience reductions in PM$_{2.5}$. Another region with reductions greater than $1 \mu g/m^{-3}$ occurs in the US eastern seaboard corridor. Significantly, these regions do not coincide with the regions of largest NH$_3$ emission reductions (cf. Fig. 4). The San Joaquin valley of central California also shows seasonal average PM$_{2.5}$ reductions greater than $0.5 \mu g\,m^{-3}$ and locally as large as $2 \mu g\,m^{-3}$. The Vancouver to Seattle region close to the western border of the model domain has PM$_{2.5}$ reductions up to $1.5 \mu g\,m^{-3}$ in the summer; this effect is highly seasonal however, with a reduction of only $0.25 \mu g\,m^{-3}$ in the winter and intermediate reductions in the transition seasons. The Alberta-Saskatchewan area of western Canada has smaller reductions in PM$_{2.5}$, on the order of 0.25 to $0.5 \mu g/m^{-3}$, with the greatest reductions in the spring and fall.

The seasonal change in PM$_{2.5}$ ammonium, sulphate and nitrate mass resulting from the reduction in ammonia emissions is shown in Figs. 6, 7 and 8, respectively. Of the three inorganic components, particle nitrate accounts for the largest fraction of the total change in particle mass, fol-

lowed by ammonium, then sulphate (note that the scales change between the figures). Individual particulate species show a stronger seasonal variation than does the total particle mass: the greatest reductions in ammonium and nitrate mass (Figs. 6, 8) occur in spring, summer and fall, while the greatest reductions in sulphate mass (Fig. 7) occur in fall, winter and spring. Particle sulphate is predicted to *increase* slightly in the summer (Fig. 7, upper left panel, blue region) in much of eastern North America following the reduction in ammonia gas emissions. This increase in sulphate, however, is more than compensated by the decreases in ammonium and nitrate, with the net result that the total PM$_{2.5}$ mass in the summer decreases in the same region (Fig. 5, upper left panel). The spatial distribution of the mass reductions also varies between the species: ammonium and nitrate reductions occur largely in regions downwind of the main ammonia emitting areas (compare to Fig. 2), whereas particle sulphate reductions (in the colder three seasons of the year) are coincident with the ammonia emitting regions.

Our interpretation of these results is as follows:

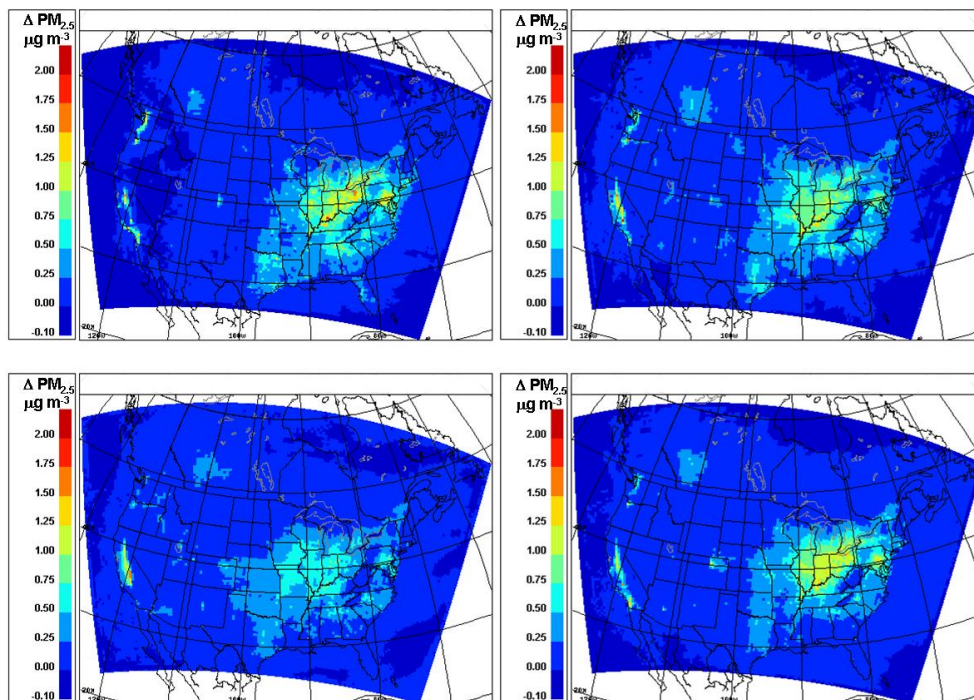(1) Most of the reduction in PM$_{2.5}$ mass is due to decreases in ammonium and nitrate mass.

Fig. 5. Seasonal average change in PM$_{2.5}$ mass, μg m^{-3}, associated with a 30% reduction in agricultural NH$_3$ emissions. Reductions in PM$_{2.5}$ are shown as positive values. Panels arranged as in Fig. 2.
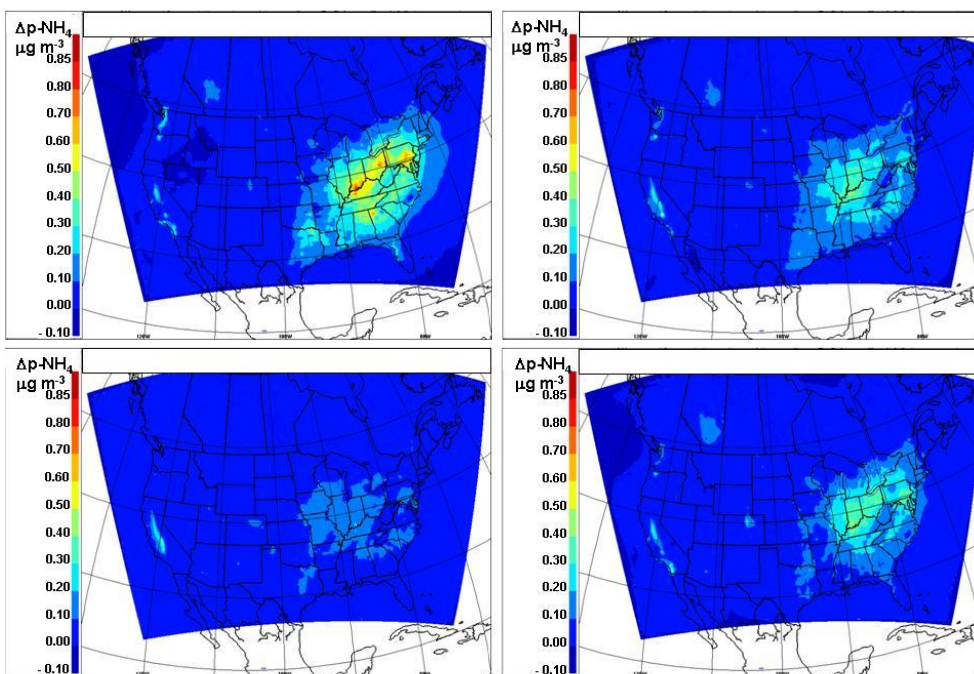

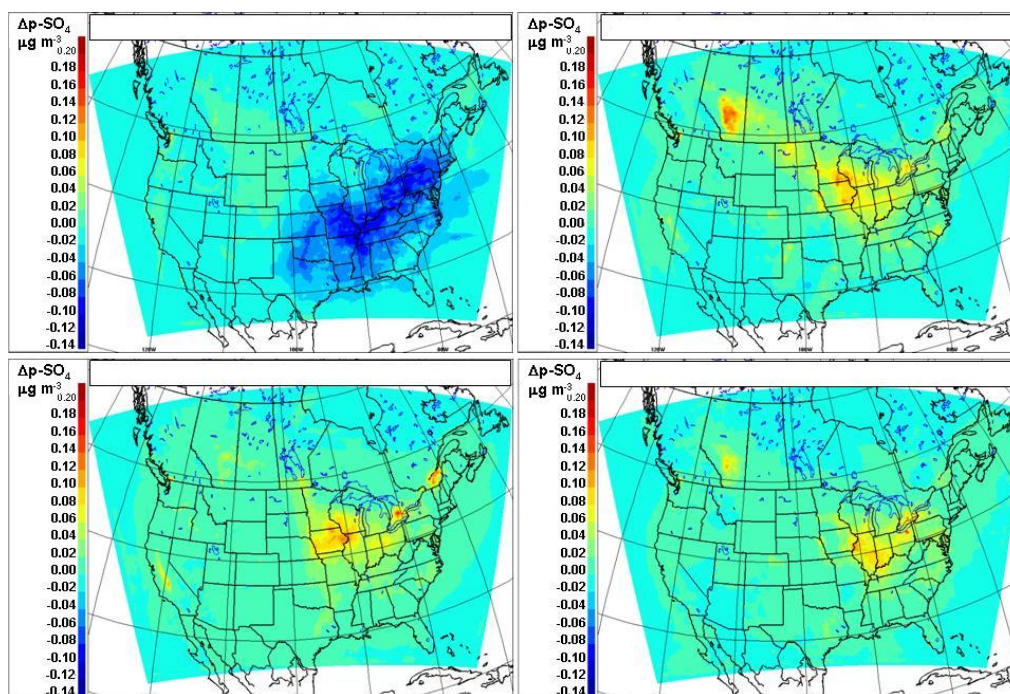**Fig. 6.** Same as for Figure 5, but for the p-NH$_4$ component of PM$_{2.5}$.

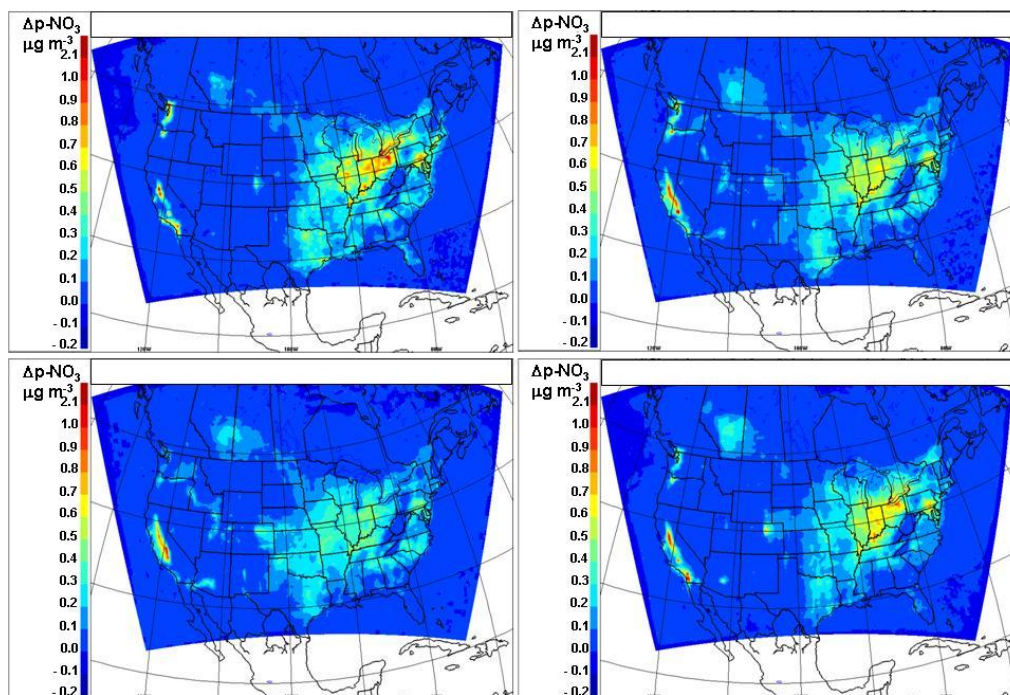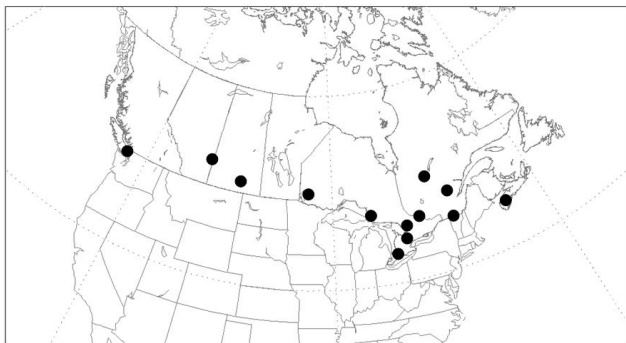**Fig. 7.** Same as for Fig. 5, but for the p-SO$_4$ component of PM$_{2.5}$.

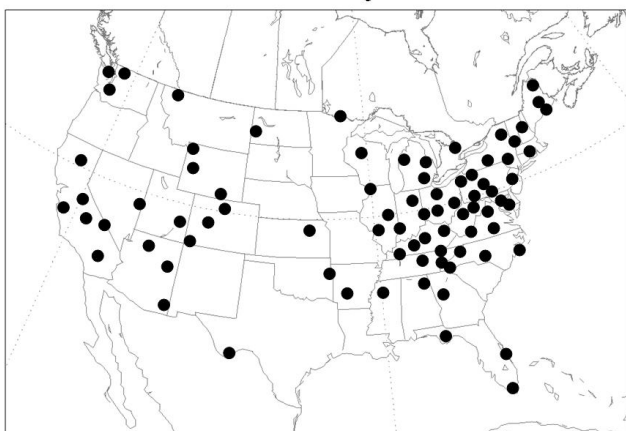**Fig. 8.** Same as for Fig. 5, but for the p-NO$_3$ component of PM$_{2.5}$.

Fig. 9. Locations of sites used in analysis of episodic nature of ammonia emissions reductions: **(a)** Canadian CAPMoN sites; **(b)** US CASTNet sites.
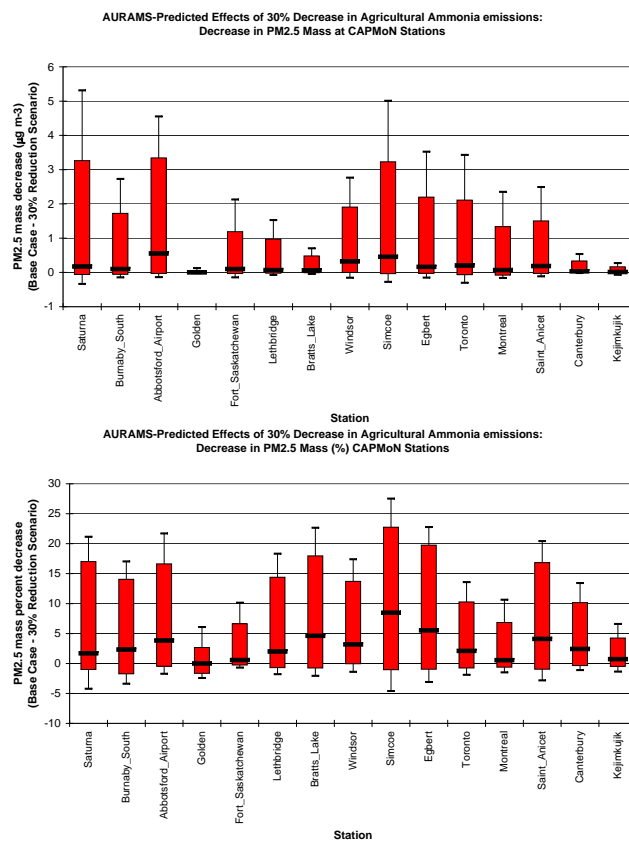

Fig. 10. AURAMS-predicted annual frequency distributions of the decrease in hourly $PM_{2.5}$ concentrations associated with a 30% decrease in NH_3 emissions at CAPMoN stations (numbered sites from Fig. 9a): **(a)** expressed in mass units; **(b)** Expressed as percentage difference relative to the base case. Median : solid horizontal bar; 5th and 95th percentiles: limits of red vertical bar; 2nd and 98th percentiles: thin horizontal bars.

(2) Cold-month decreases in sulphate, co-located with the ammonia emissions regions, are due to (a) increased hydrogen ion concentrations in cloudwater, which causes the $SO_2(g) + H_2O \rightleftharpoons H^+(aq) + HSO_3^-(aq)$ equilibrium to shift to the left, reducing further uptake of sulphur into clouds, (b) a decrease in the rate of cloudwater oxidation of $HSO_3^-(aq)$ to $SO_4^{2-}(aq)$ by ozone due to increased $H^+(aq)$ concentrations.

(3) The small summer increases in particle sulphate concentration result from the conversion of $HSO_3^-(aq)$ to $SO_4^{2-}(aq)$ becoming more efficient at higher hydrogen ion concentrations and higher temperatures: the aqueous phase oxidation rates of HSO_3^- (aq) to SO_4^{2-} (aq) by hydrogen peroxide and organic peroxides are proportional to the $H^+(aq)$ concentration, which increases as ammonia decreases (e.g. Fung et al., 1991). This increased irreversible conversion of $HSO_3^-(aq)$ to $SO_4^{2-}(aq)$ counteracts the cold-month equilibrium between $SO_2(g)$ and $HSO_3^-(aq)$, allowing the net uptake of SO_2 in clouds to increase. This effect occurs where the base case $H^+(aq)$ concentration was already high (i.e. the ozone oxidation pathway was already weak, due to high $H^+(aq)$ concentrations, and is weakened further by the increase in acidity).

The episodic nature of the changes in $PM_{2.5}$ mass resulting from ammonia emissions reductions has been examined by constructing annual frequency distributions of hourly mass difference and hourly percent mass difference between the base case and the 30%-reduction scenario. Hourly model values of the changes in $PM_{2.5}$ were first extracted for those model grid cells containing the CAPMoN and CASTNET monitoring stations shown in Fig. 9 and were then used to construct annual frequency distributions of hourly mass change (Figs. 10a, 11a) and percent mass change (Figs. 10b, 11b). In both Figs. 10 and 11, the sites are arranged roughly from the west of the continent on the left to the east of the continent on the right, and positive values indicate *reductions* relative to the base case. Both figures show that median hourly $PM_{2.5}$ reductions are usually less than $1\,\mu g\,m^{-3}$, or on the order of 5% of the $PM_{2.5}$ mass at any given location, while the reductions during episodes (e.g. 95th percentiles, top of red bar) may be considerably higher. For the Canadian
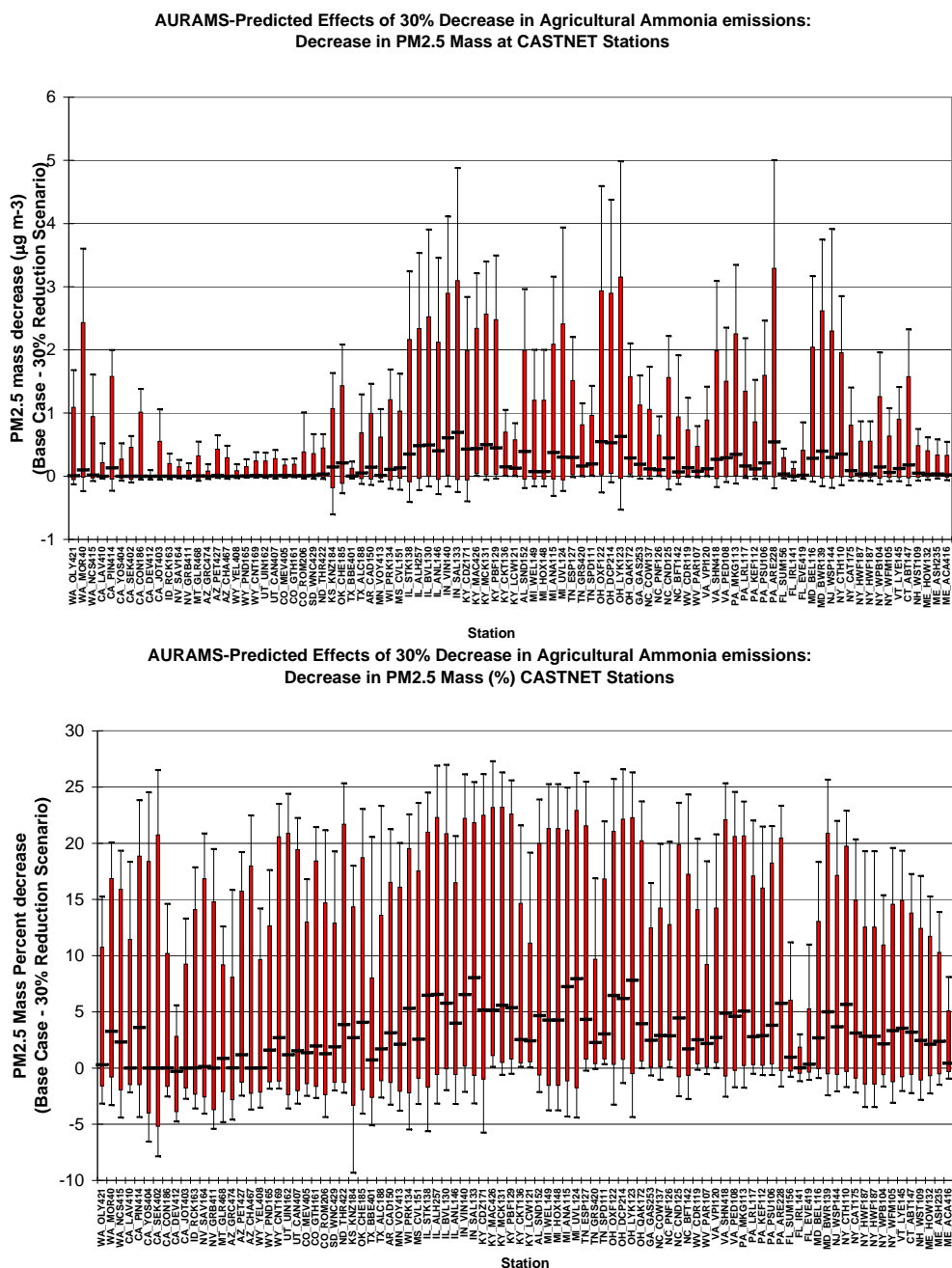
AURAMS-Predicted Effects of 30% Decrease in Agricultural Ammonia emissions:
Decrease in PM2.5 Mass at CASTNET Stations

AURAMS-Predicted Effects of 30% Decrease in Agricultural Ammonia emissions:
Decrease in PM2.5 Mass (%) CASTNET Stations

Fig. 11. (a) Same as Fig. 10a but for CASTNet station sites shown in Fig. 9. (b) Same as Fig. 10b but for CASTNet station sites shown in Fig. 9.

sites (CAPMoN), the largest median mass reductions (Figure 10a) are at Abbotsford Airport ($0.55\,\mu\mathrm{g\,m^{-3}}$) located in an agricultural area to the east of Vancouver, British Columbia, and Simcoe, Ontario, located in an agricultural area to the east of the Detroit/Windsor conurbation ($0.50\,\mu\mathrm{g\,m^{-3}}$). The median values at all sites are much lower than the 95th-percentile limits (e.g., Abbotsford Airport, 95th percentile value of $3.3\,\mu\mathrm{g\,m^{-3}}$; Simcoe, $3.2\,\mu\mathrm{g\,m^{-3}}$). Median percent

reductions (Fig. 10b) are more centered in the frequency distributions, although the upper ends of the range are still considerably higher than the medians (e.g., Abbotsford Airport median and 95th-percentile values of 3.8% and 17%; Simcoe 8.5% and 23%, respectively). A similar pattern may be observed at US sites (CASTNET), with median and 95th mass percentile values in Indiana and Ohio reaching 0.69 and $3.1\,\mu\mathrm{g\,m^{-3}}$, and 0.63 and $3.2\,\mu\mathrm{g\,m^{-3}}$ respectively, and
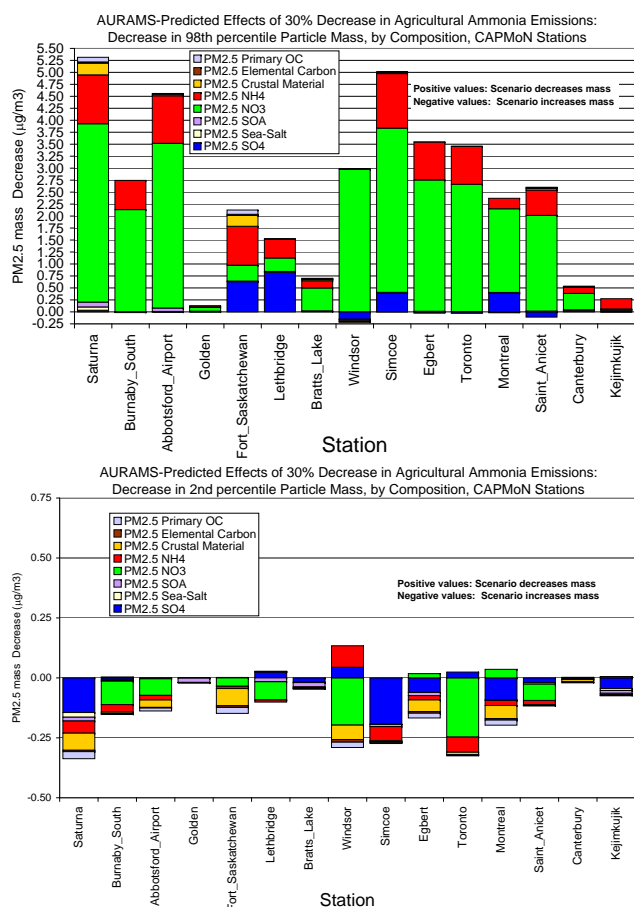
Fig. 12. AURAMS-predicted PM$_{2.5}$ composition change associated with a 30% decrease in NH$_3$ emissions at CAPMoN statons for **(a)** the 98th percentile PM$_{2.5}$ mass change at each station, and **(b)** the 2nd percentile mass change at each station. Note the difference in vertical scale between (a) and (b).

corresponding percent reduction median and 95th-percentile values of 8% and 22%, and 7.8% and 22%, respectively. The mass reduction distributions (Figures 10a, 11a) suggest that the impact of ammonia controls on PM$_{2.5}$ mass will be episodic, with mass reductions during periods of elevated PM$_{2.5}$ levels being as much as 4 to 6 times greater than the median mass reduction. The percent mass reduction distributions (Figs. 10b, 11b) show that median percent mass decreases of 0 to 8% are predicted at the network locations in both countries, with 95th-percentile values of up to 22%. However, Figs. 10 and 11 also show that NH$_3$ emission decreases can also lead to lower-magnitude episodic increases of PM$_{2.5}$ mass.

The speciation of the change in particle mass for the 98th and 2nd percentile PM$_{2.5}$ mass changes from Figures 10 and 11 are shown in Figs. 12 and 13, respectively. This analysis shows that the large decreases in PM$_{2.5}$ mass (98th percentile; Figs. 2a and 13a) are mostly due to decreases in par-

ticle ammonium and particle nitrate mass, in accord with the seasonal average concentration diagrams discussed above. The small decreases in PM$_{2.5}$ mass (2nd percentile, Figs. 12b and 13b) show a variety of causes in Canada (12b), but in the eastern USA. they are clearly linked with the increase in sulphate mass noted in the analysis above in the summer months, particularly in the eastern United States of America (13b). It is interesting to contrast these sulphate results with those of Tsimpidi et al. (2008): in their case, a 50% reduction in ammonia emissions for an eastern US domain resulted in minor sulphate reductions in a single winter month, and no change in sulphate in a single summer month. Our trend is the same, though we predict small sulphate *increases* in the summer due to the impact of increased cloudwater acidity on aqueous-phase oxidation processes, described above. The differences between our results and those of Tsimpidi et al. (2008) may relate differences in the equilibrium and reaction rate expressions used in the two different models, and in the temperatures during the respective test periods. Other small decreases may be due to reductions in ammonia emissions upwind of the site leading to less particle growth and hence to less particle dry deposition prior to reaching the downwind site (i.e. extreme cases where the base case particle ammonium nitrate is sufficiently high that some particle nitrate is lost en-route to the measurement station location).

4.2.3 PM$_{2.5}$ chemistry

The manner in which the reductions in NH$_3$ emissions create the PM$_{2.5}$ mass reductions described above can be examined by considering the changes in the metrics of Table 3.

The predicted change in particle neutralization ratio resulting from a 30% reduction in NH$_3$ emissions relative to the base case is shown in Fig. 14. Positive regions indicate areas where the neutralization ratio has *decreased* (i.e., the particles have become more acidic) compared to the base case, and negative regions indicate areas where the neutralization ratio has *increased* (i.e., the particles have become less acidic). The main NH$_3$ emitting regions in the US midwest display relatively little change in particle charge balance; these regions are NH$_3$-saturated, so there is little impact on particle charge balance in spite of the predicted concurrent decreases in ambient NH$_3$ concentrations (cf. Fig. 4). Substantial decreases in the particle neutralization ratio (i.e., increases in particle acidity and changes in particle composition) do occur downwind and on the fringes of the NH$_3$ emissions regions.

The predicted change in the total ammonium to sulphate mole ratio resulting from the 30% change in NH$_3$ emissions is shown in Fig. 15. The total ammonium to sulphate ratio describes the chemical regime, and Figure 15 shows that the reduction in emitted NH$_3$ has resulted in a more acidic chemical regime over the NH$_3$ source regions, with relatively little change outside of those source regions. Figures 14 and 15 suggest that the composition of particles formed over the
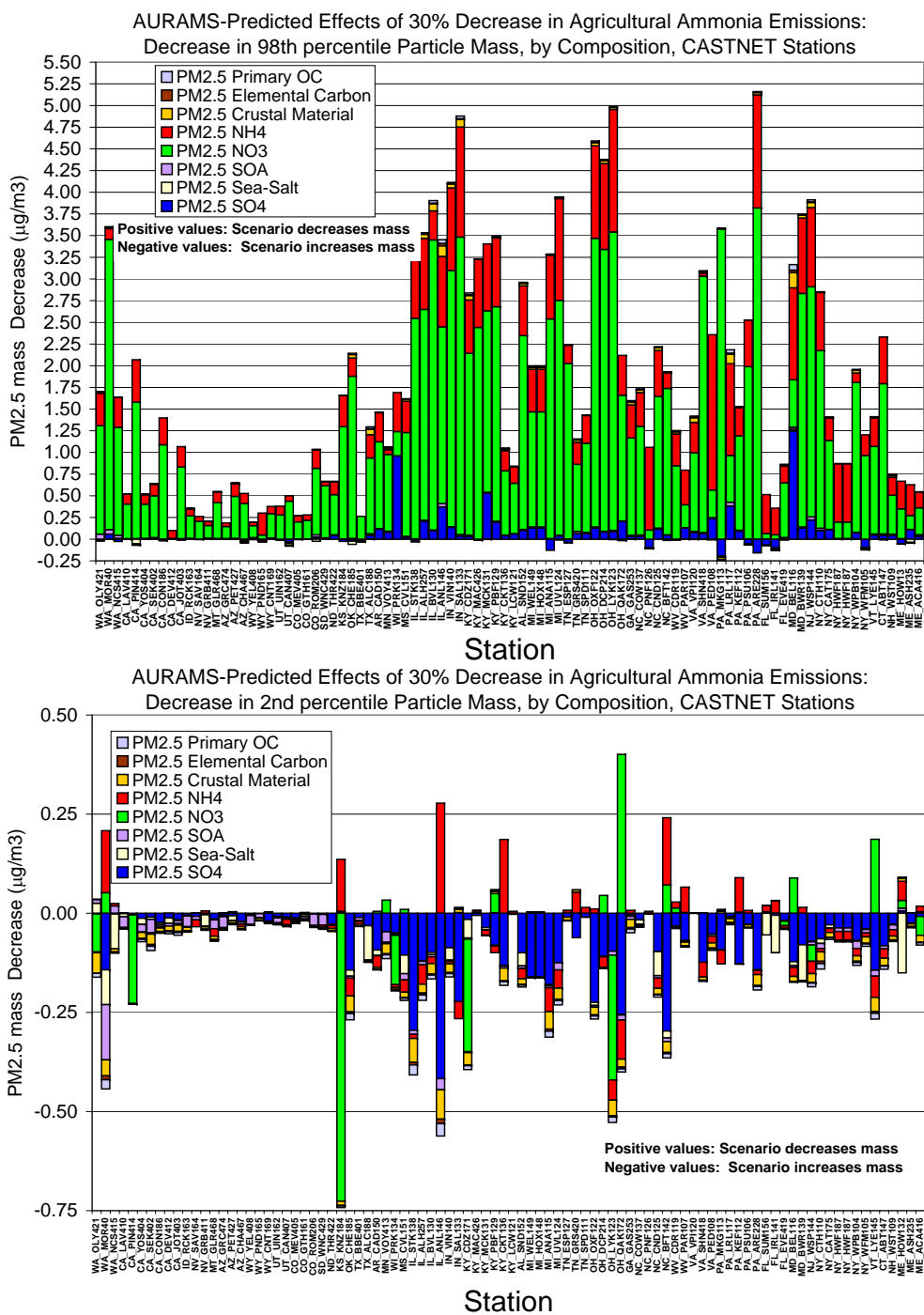
AURAMS-Predicted Effects of 30% Decrease in Agricultural Ammonia Emissions:
Decrease in 98th percentile Particle Mass, by Composition, CASTNET Stations

AURAMS-Predicted Effects of 30% Decrease in Agricultural Ammonia Emissions:
Decrease in 2nd percentile Particle Mass, by Composition, CASTNET Stations

Fig. 13. (a) Same as Fig. 12, for CASTNet stations. **(b)** Same as Fig. 12, for CASTNet stations.

NH_3 source regions will change. For example, given the minor change in neutralization ratio in southern Minnesota (Fig. 14), the drop in total ammonium to sulphate mole ratio in these regions (Fig. 15) suggests that the particles may have more acidic components (hydrogen ion, etc.) over the source regions. That is, these two figures taken together suggest that particle nitrate is the dominant means of transport of NH_3 from the source regions to regions downwind; the mass of particle sulphate in the NH_3 source regions is invariant, and the lack of change in the neutralization ratio there shows that reductions in particle ammonium are being accompanied by reductions in particle nitrate (see Figs. 6 and
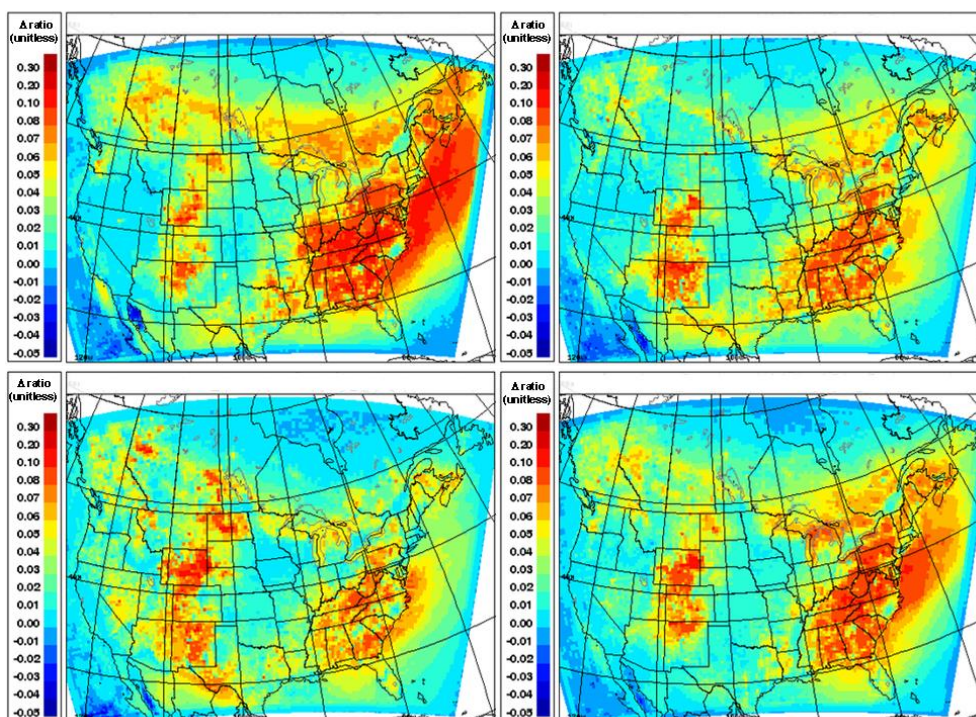
Fig. 14. Change in particle neutralization ratio due to 30% reduction in NH$_3$ emissions. Positive regions indicate increased particle acidity relative to the base case. Panels arranged as in Fig. 2.

8). The downwind impact of the NH$_3$ emissions is therefore due in part to particle ammonium nitrate transport.

A strong seasonal variation in changes to chemical regime can also be seen in Fig. 15, particularly over the Canadian Prairies. Spring and fall have the greatest increase in particle regime acidity, while summer and winter have smaller changes.

The change in the mass fraction of NH$_3$ (i.e., $[NH_3(g)]\big/\{[NH_3(g)] + [PM_{2.5}-NH_4]\}$ on a mass basis) is shown in Fig. 16. The differences are positive over most of the domain and over all seasons, showing that a greater *proportion* of the remaining (ammonia + ammonium) mass resides in the particle phase instead of the gas phase following a reduction in NH$_3$ emissions. The effect is strongest in the summer and weakest in the winter. The figure suggests that reductions in NH$_3$ gas emissions will result in a nonlinear reduction in NH$_3$ gas concentrations due to thermodynamics: a shift in phase will reduce the *relative* amount of NH$_3$ that remains in the gas-phase.

The ratio of the sum of PM$_{2.5}$ nitrate and ammonium mass to total PM$_{2.5}$ mass is shown in Fig. 17. This figure shows that the relative amount of PM$_{2.5}$ composed of these NH$_3$-sensitive species has decreased in the 30% reduction scenario. The figure is also of interest in that it confirms ammonium nitrate as the means of long-range transport of NH$_3$ mass. Comparing the summer (upper left) panels of Figs. 17, 4, and 5, it can be seen that:

1. The largest ammonia source region is located in southern Minnesota and northern Iowa (Fig. 4), while the largest particle mass reductions occur further to the east, north of the Ohio River (Fig. 5).

2. The region of greatest particle ammonium and nitrate reduction (Figs. 6, 8 and 17) occurs over the state of Illinois i.e., between the ammonia source region and the region of greatest particle mass reduction.

The change in the fraction of directly NH$_3$-sensitive particle mass has a strong seasonal variation, with the greatest impact in the winter (lower left panel, Fig. 17). This is consistent with the strong dependence of particle nitrate formation on temperature, with colder temperatures resulting in a greater proportion of ammonia and nitric acid gas being converted to particle ammonium nitrate, ammonium, and nitrate ions.

4.2.4 Total deposition

AURAMS calculates the wet and dry deposition of various species to the Earth's surface as moles m^{-2} hour^{-1}. The hourly wet and dry deposition fields have been added together and summed to seasonal mass totals (kg/ha/season) for the following analysis. As before, scenario values are then subtracted from the base case to determine the impact of the reduced NH$_3$ emissions.
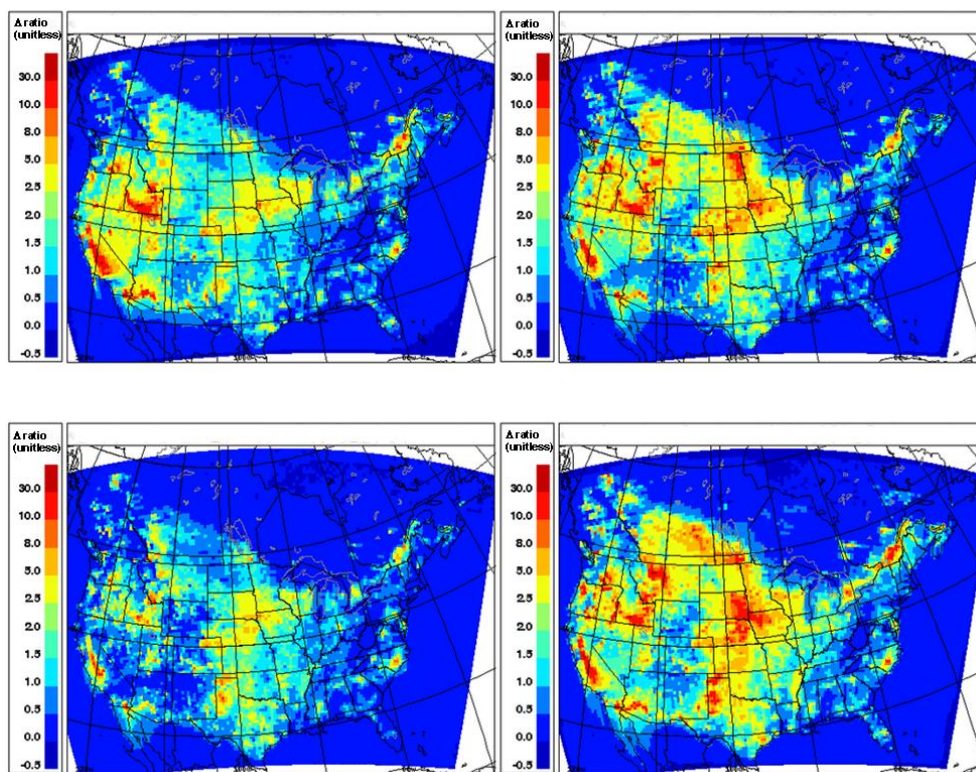
Fig. 15. Change in total ammonia to sulphate mole ratio due to 30% reduction in NH$_3$ emissions. Positive regions indicate decreases in the ratio (more acidic chemical regimes) relative to the base case. Panels arranged as in Fig. 2.

The predicted change in total deposition of all forms of sulphur (SO$_2$ + H$_2$SO$_4$ + p-SO$_4$ dry deposition and wet deposition) is depicted in Fig. 18. The 30% reduction in the emissions of NH$_3$ has resulted in decreases in sulphur total deposition (red) in many regions in both Canada and the USA.. Increases in sulphur deposition are also present, in the colder seasons (SE US, Atlantic provinces). It should be noted that these predicted changes to the sulphur deposition associated with ammonia emissions reductions, while significant, are relatively small in magnitude relative to the total sulphur deposited: on the order of 1% of the total sulphur total deposition.

The predicted changes in sulphur total deposition are the result of the following NH$_3$ emissions-reduction-induced changes in the state of atmospheric sulphur:

1. A reduction in NH$_3$ reduces the capacity of cloud water and rain to absorb SO$_2$, via the net equilibrium: NH$_3$(g) + SO$_2$(g) + H$_2$O $\Leftrightarrow$ NH$_4^+$(aq) + HSO$_3^-$(aq).

The concentration of the ammonium ion decreases, hence less SO$_2$(g) can enter the aqueous phase as HSO$_3^-$(aq) in the absence of the buffering provided by NH$_3$. The reduction of

the sulphur content in cloud water and rain results in less sulphur being removed by wet deposition. Note that in the presence of higher temperatures and sufficient aqueous-phase oxidation of HSO$_3^-$(aq), this equilibrium will shift to the right (see discussion above in section 4.2.2).

1. A corollary to (1) is that less sulphur is removed in precipitation. The sulphur, which remains in the form of SO$_2$(g), will therefore be transported longer distances due to decreased rainout/washout. The increases in sulphur deposition that takes place in the colder seasons in Fig. 18 (eastern seaboard of US, Atlantic Ocean) results from the transport and subsequent deposition of SO$_2$ to greater downwind distances.

2. Another corollary to (1) is that reductions in NH$_3$ emissions will reduce the amount of ammonium ion in the cloud droplets and water, and hence will reduce the amount of nitrate taken up in cloud water and rain, and thus the amount of nitrate removed by wet deposition. Total nitrogen deposition therefore decreases due to decreases in both reduced and oxidized nitrogen deposition, as discussed below.
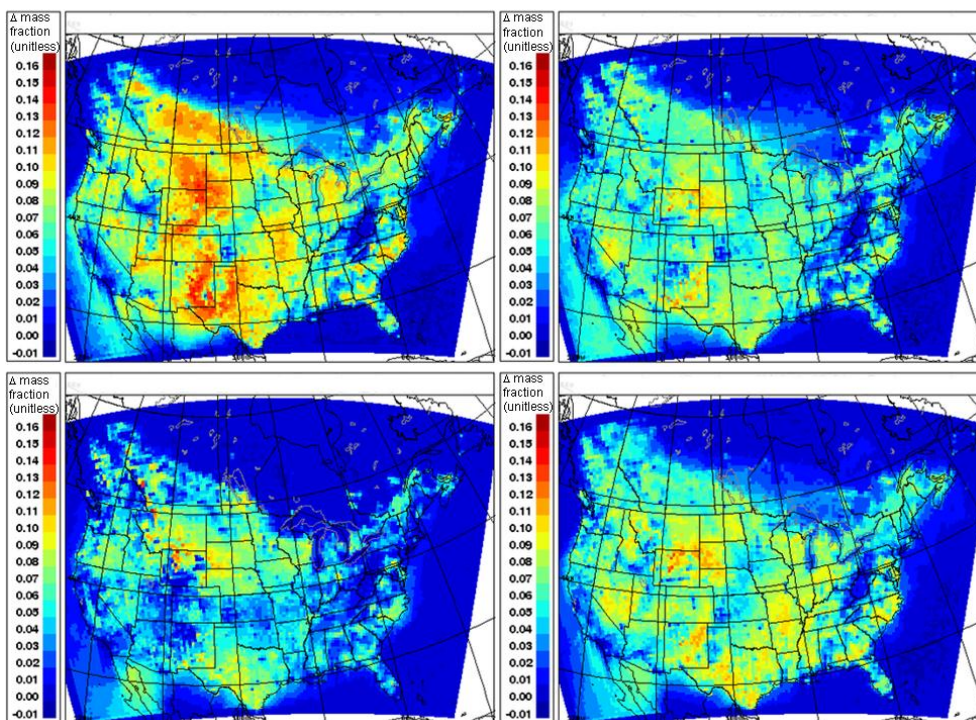
Fig. 16. Change in gas-phase NH$_3$ mass fraction due to 30% reduction in NH$_3$ emissions. Positive regions indicate decreases in mass fraction (i.e., proportionately more ammonium in the particle phase) relative to the base case. Panels arranged as in Fig. 2.
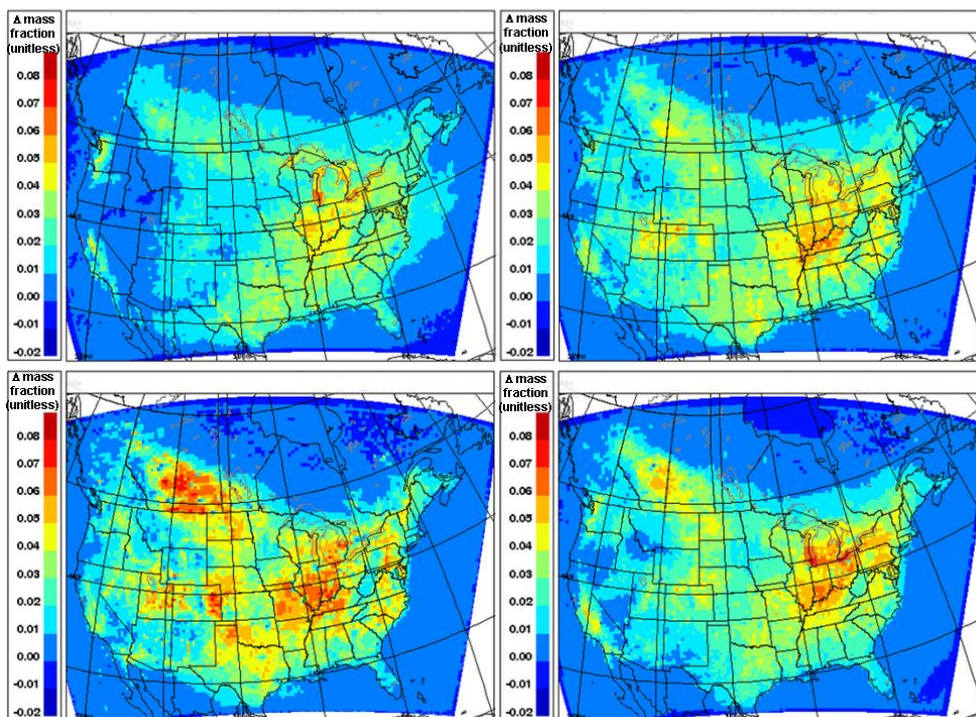
Fig. 17. Change in fraction of ammonium + nitrate mass in PM$_{2.5}$ relative to the total PM$_{2.5}$ mass. Positive regions indicate decreases in ammonium and nitrate mass fraction (i.e., particles composed of proportionately less ammonium and nitrate) relative to the base case. Panels arranged as in Fig. 2.
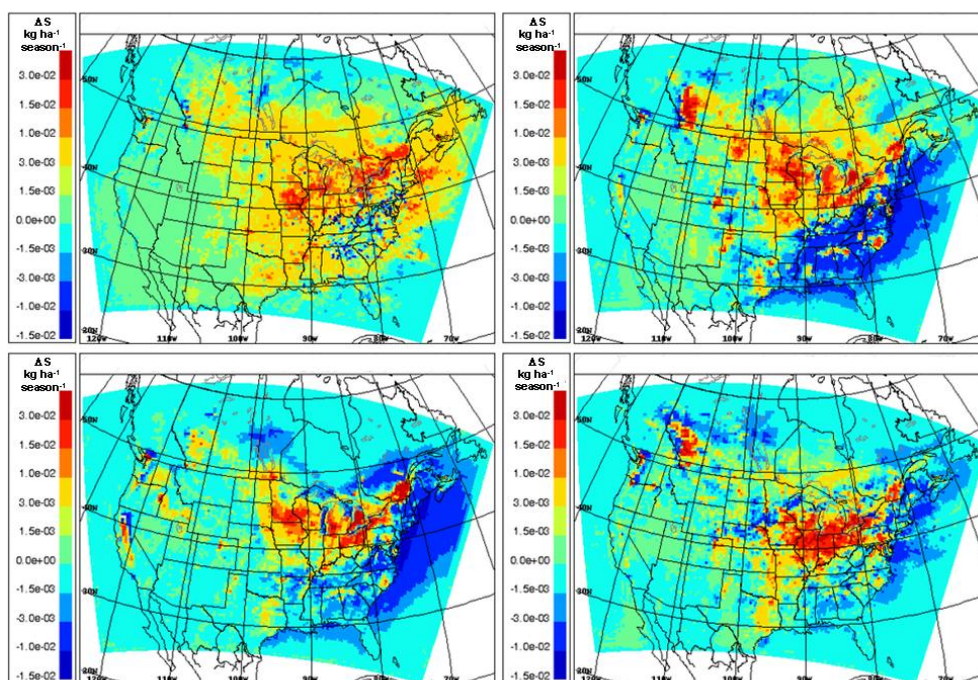
Fig. 18. Change in total – sulphur total deposition (kg S/ha/season) due to 30% reduction in NH$_3$ emissions. Positive values (green to red colours) indicate decreases in sulphur deposition resulting from decreasing NH$_3$ emissions; negative values (blue) indicate increases in sulphur deposition resulting from decreasing NH$_3$ emissions. Panels arranged as in Fig. 2.
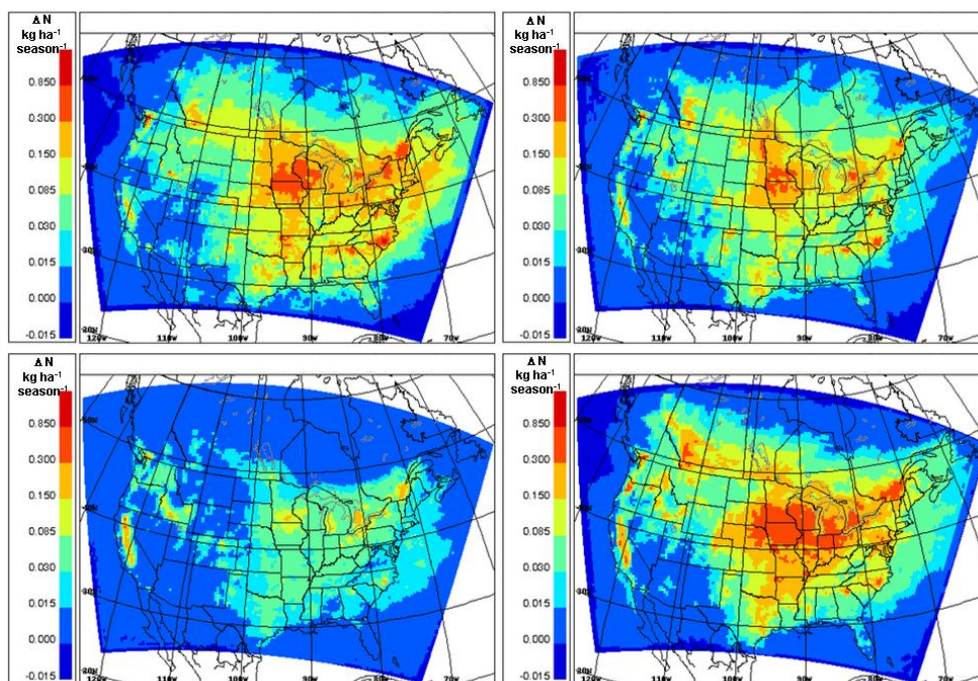
Fig. 19. Change in total – nitrogen total deposition (kg N/ha/season) due to 30% reduction in NH$_3$ emissions. Positive values (light blue to red colours) indicate decreases in nitrogen deposition resulting from decreasing NH$_3$ emissions; negative values (dark blue) indicate increases in nitrogen deposition resulting from decreasing NH$_3$ emissions. Panels arranged as in Fig. 2.

3. Reductions in NH_3 emissions may also cause a reduction in the size of ambient particles, since less NH_3 leads to less p-NH_4 and p-NO_3 in the particle phase, hence smaller particles, which may have a smaller deposition velocity.

The change in total deposition of all phases of nitrogen related to ammonia chemistry (sum of $\{NH_4^+(aq) + NH_3(g) + PM_{2.5}\ NH_4 + NO_3^-(aq) + HNO_3(g) + PM_{2.5}\ NO_3\ \})$ is shown in Fig. 19. The reduction in NH_3 emissions by 30% has resulted in substantial reductions in deposited nitrogen (similar in magnitude to the total deposited nitrogen in many locations). The greatest spatial extent of nitrogen deposition reduction occurs in the spring (lower right panel), when NH_3 emissions are highest, and the smallest change occurs in the winter (lower left panel), when NH_3 emissions are lowest. The location of the largest reductions in nitrogen deposition occurs over the NH_3 emitting areas (compare Figs. 4 and 19. Less than 10% of the total change in deposited nitrogen is associated with the various forms of nitrate, and is instead dominated by the ammonium components (not shown). The change in total ammonia/um deposition is itself dominated by aqueous ammonium wet deposition (approximately 5/6 of the total) and NH_3 dry deposition (remaining 1/6), with changes to p-NH_4 dry deposition being relatively insignificant for the nitrogen budget.

The main results of the deposition analysis for a 30% reduction in agricultural NH_3 emissions are thus:

1. Sulphur deposition close to the sources of sulphur decreases slightly, due largely to a reduction in $SO_2(g)$ uptake in clouds. Sulphur deposition further downwind of the sources may increase as a consequence, depending on the season.

2. Nitrogen deposition decreases significantly, driven largely by decreases in aqueous ammonium wet deposition (75% of the total decrease in N) and dry deposition of ammonia gas (15%), but also by near-source decreases in deposition of all forms of nitrate (10%).

3. Hydrogen ion wet deposition increases (not shown). The increase in hydrogen ion deposition is spatially matched with the decreases in nitrogen deposition and is greatest over the regions of NH_3 emissions.

4.2.5 Annual critical load exceedances for sensitive ecosystems

Annual critical-load exceedance fields for Canada were calculated for the base case and for the 30% emissions reduction scenario in two ways: for (a) sulphur (S) total deposition and for (b) sulphur + nitrogen (S + N) total deposition.

Annual critical-load exceedances for sulphur were not significantly changed between the base case and the 30%

NH_3 emissions reduction scenario (annual critical-load exceedances did decrease for the NH_3 emissions reduction scenario, but significant reductions only occurred at two model gridpoints: not shown). This indicates that the impact of NH_3 emissions reductions on sulphur acidification of ecosystems is expected to be small, in accord with the relatively small changes in total sulphur deposition (Fig. 18).

Figure 20a shows the predicted S + N annual critical-load exceedances for the base case. Figure 20b shows the corresponding reductions in S + N annual critical-load exceedances in many parts of Canada that are predicted to result from a 30% reduction in agricultural NH_3 emissions. These substantial decreases in S + N annual critical-load exceedances are in contrast to the small decreases in S-only annual critical-load exceedances.

The implication of this finding is that if an ecosystem's ability to absorb N from atmospheric deposition is compromised at these locations in the future, i.e., N saturation (e.g., Aber and Magill, 2004), then the deposition of atmospheric nitrogen resulting from NH_3 emissions will contribute to a degradation of these ecosystems. While recent streamwater-chemistry trend analyses in Europe suggest that many decades of elevated N deposition may be required for N saturation to occur (Wright et al., 2001), reduced N retention in soils and increased N leaching to streams and lakes can begin much sooner (e.g., Kaste et al., 2002; Jeffries and Ouimet, 2005). Reductions in NH_3 emissions can thus reduce present or potential acidification due to inorganic N deposition

4.2.6 A conceptual model

The above analysis of AURAMS simulations may be used to provide a simple conceptual model to describe the effect of reductions in NH_3 emissions on atmospheric chemistry. The following diagram (Figure 21) depicts the processes, on a hypothetical transect with NH_3 emissions on the left, a source of SO_2 and NO_x in the centre, and a receptor region downwind on the right. This is similar to the situation on the eastern half of the North American continent, with the US midwest NH_3 source on the left, the Ohio Valley and Great Lakes regions in the centre, and the Atlantic provinces and New England states on the right. The prevailing wind blows from left to right in this diagram. The upper half of the diagram shows the system in the absence of NH_3 emission controls, the lower half the system including controls in NH_3 emissions. Coloured text in the lower half of the diagram indicates terms that have changed; red for species that have decreased, blue for species that have increased, and green for species with a non-linear response that may be seasonally dependant.

In the absence of emissions controls (Figure 21, top), excess NH_3 in the source region at left creates particle ammonium nitrate, in addition to particle ammonium sulphate. Winds blowing to the right then transport the particles and
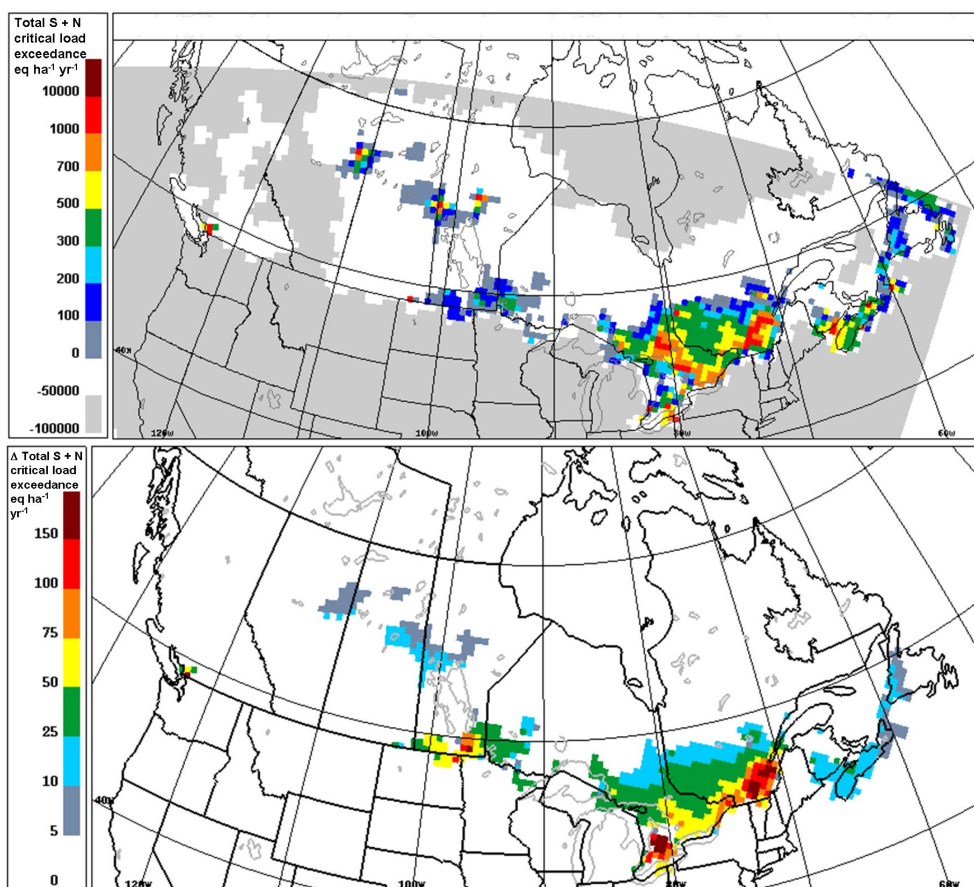
Fig. 20. AURAMS-predicted Canadian (S + N) critical-load exceedances for 2002: (top) NAESI base case; and (bottom) (base case – 30% NH$_3$ emissions reduction scenario). Gray areas in the top panel indicate areas for which critical-load values were not available. Positive values in the bottom panel indicate areas where the critical load exceedance has *decreased* in response to decreasing NH$_3$ emissions.

NH$_3$ gas. En route, the NH$_3$ gas is depleted due to wet and dry deposition, as are the particles by wet deposition. Nevertheless, significant amounts of particle ammonium and nitrate reach the SO$_2$ and NO$_x$ emissions source region in the centre of the figure. The addition of fresh SO$_2$ and nitric acid to the system cause the particles to locally become more acidic, with some transfer of the transported ammonium from particle nitrate to particle sulphate possible due to inorganic thermodynamics. With subsequent transport further downwind, the particles are deposited; relatively little SO$_2$ reaches far downwind locations due to NH$_3$-enhanced aqueous-phase conversion to sulphate closer to the source regions, particularly in colder seasons, when HSO$_3^-$(aq) oxidation is inhibited.

With the presence of NH$_3$ controls (Figure 21, bottom, also Figs. 5, 6, 7, 8, 12, 13), less ammonium nitrate is created in the Midwest source region, and hence less is available for transport (e.g. Fig. 8, seasonal average p-NO$_3$ decreases of $>0.7 \mu$g/m^{-3} in western Illinios, summer and fall). Smaller amounts of ammonium reach the central SO$_2$

and NO$_x$ source region; this reduces the rate of further particle formation and allows more subsequent downwind transport and deposition of SO$_2$. (see Fig. 6, note p-NH$_4$ decreases in NW Illinios, NW Indiana of about 0.2 μg/m^{-3}, also note Fig. 18b, c, sulphur deposition increasing fall and winter, when aqueous phase conversion to sulphate is less efficient; more transport of SO$_2$ and less deposition close to sources). Depending on the season, the conversion of HSO$_3^-$(aq) to SO$_4^{2-}$(aq) in cloud water may increase with the drop in H$^+$(aq) associated with ammonia emissions increases. (see Fig. 7a, average summer increase in p-SO$_4$ over the Eastern USA. on the order of 0.10 μg/m^{-3}, due to cloud water oxidation of SO$_2$).

A neutral charge balance ratio is maintained over the NH$_3$ source region at the left regardless of the scenario; since this region remains NH$_3$-saturated, reductions in p-NH$_4$ here are matched by reductions in p-NO$_3$ in the denominator (c.f. Figure 14, neutralization over Minnesota and Iowa is unchanged despite emissions reductions). In the SO$_2$ and NO$_x$ source region in the centre, however, the upwind reductions in NH$_3$

Fig. 21. Conceptual model of NH_3 emissions, reaction and transport: (top) without NH_3 emissions controls; (bottom) with NH_3 emissi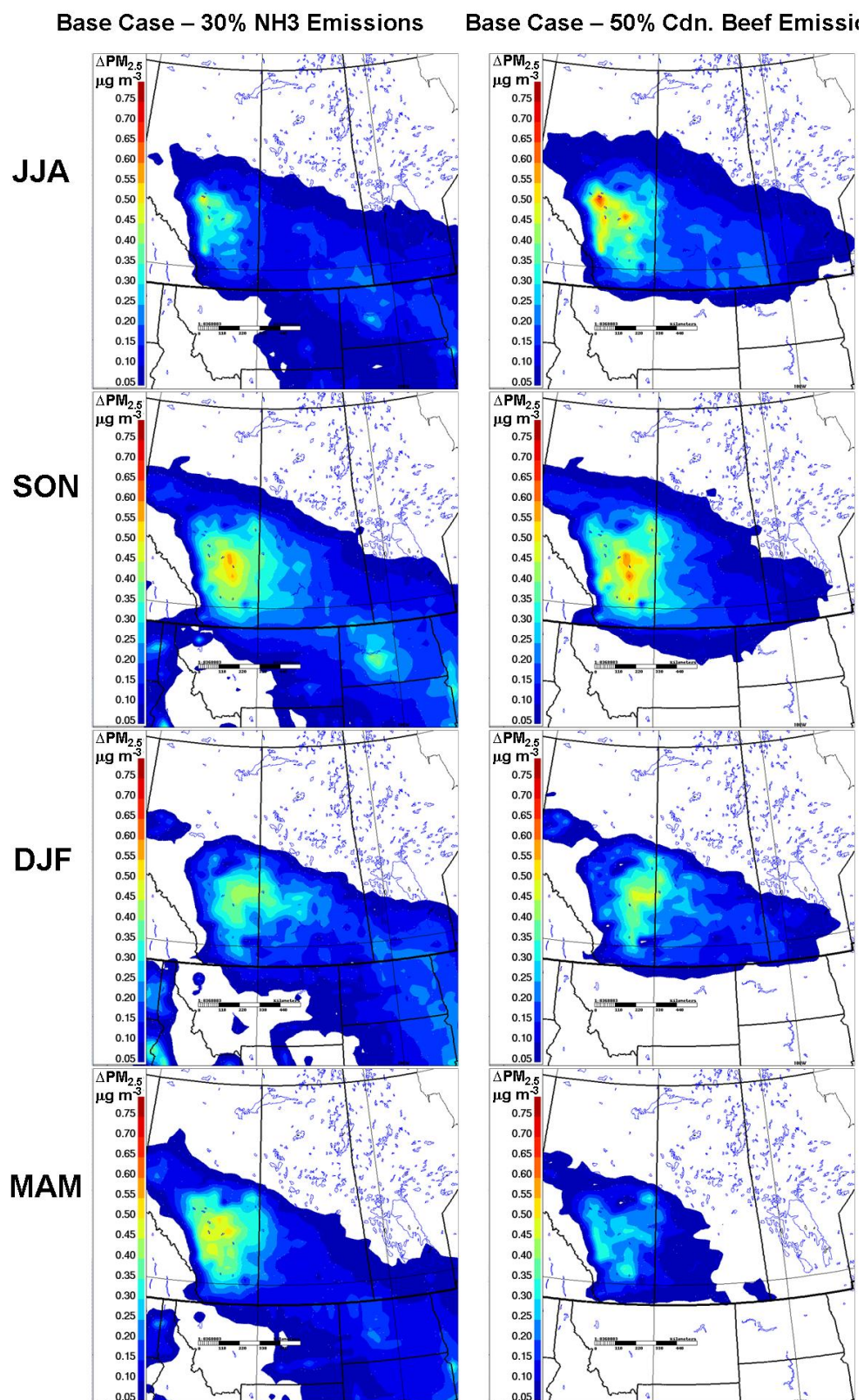ons controls. Font colours: red: species that have decreased with NH_3 emissions controls; blue: species that have increased; green: species with a non-linear response that may be seasonally dependant.

emissions result in a net decrease in charge balance and an increase in particle acidity that is then maintained during further downwind transport (c.f. Figure 14, Ohio river valley increased acidity).

While this conceptual model aids in understanding the AURAMS predictions, it is not intended as a quantitative analysis of a given region, or a specific time period.

5 Uncertainty analysis of the 50% Canadian Beef Cattle emissions reduction scenario

The main intent of this scenario was to serve as an uncertainty benchmark for the previous scenario. The sub-sector with the largest uncertainty in the Canadian agricultural NH_3 emissions inventory is that of Beef Cattle, estimated to be as high as a factor of two; the 50% reduction considered in this scenario thus represents the lower range of the uncertainty envelope. Comparisons to the 30% all-sector scenario thus show the limitations to the above analysis, in locations where this sub-sector dominates NH_3 emissions.

The model response for $PM_{2.5}$ mass for this emissions scenario, relative to the base case, is shown below in Fig. 22. This combines the seasonal difference in $PM_{2.5}$ due to a 30% agricultural ammonia reduction (left hand column of panels) with the seasonal difference due to a 50% reduction in ammonia emissions from Canadian Beef Cattle alone (right-hand column of panels). The reduction of beef-cattle emissions by 50% has about the same impact in this region (about the same size as the US state of Texas) as the 30% overall reduction noted above. Smaller magnitude changes were also noted in the province of Ontario (not shown).

One important conclusion from this analysis is that for the Canadian Prairie provinces, the range of uncertainty in model predictions associated with the beef-cattle emissions factors may be as large as the impacts from an across-the-board 30% reduction of NH_3 emissions. While the best available information was used to compile the new NH_3 emissions inventory, improvements in the beef-cattle subsector of the inventory are recommended for future work. Similar uncertainty analyses for US ammonia emissions are also recommended.

The other aspect to this sensitivity analysis is to demonstrate the extent to which sector-specific scenario simulations are possible with the updated 2002 NH_3 Canadian emissions inventory. An emissions reduction strategy may be "tailored" for the dominant emissions sources in a given region; very specific emissions reduction strategies may be tested in the future.

6 Conclusions and recommendations for future research

A unified regional air-quality modelling system (AURAMS) was used to investigate the effects of reductions in NH_3 emissions on regional air quality, especially PM. Three simulations of one-year duration were performed for a North American domain for different sets of NH_3 emissions. The simulation for a 30% continent-wide reduction in agricultural ammonia emissions predicted decreases in median hourly $PM_{2.5}$ mass of $<1\,\mu g\,m^{-3}$. However, the atmospheric response to these emission reductions has marked seasonal variations, and on even shorter time scales the impacts of the emissions reductions are highly episodic: for example, 95th-percentile hourly $PM_{2.5}$ mass decreases may be a factor of six larger than the median values.

A key feature of the above simulations is the manner in which continental-scale long-range transport may play a role in defining the impacts of reductions in NH_3 emissions. The emissions reductions affect local NH_3 gas concentrations, but the largest impacts of these reductions may take place significantly downwind of the main NH_3 emissions source in strongly or weakly NH_3-limited areas. The interaction between transport and chemistry is complex: NH_3 mass is transported from the source regions as aqueous and particle ammonium, and emissions of other particle precursors play a significant role in the subsequent chemistry. Reductions in NH_3 emissions result in a small but significant decrease in the amount of SO_2 gas converted to sulphate in the colder three seasons of the year. Small increases in aqueous sulphate formation and SO_2 uptake are predicted in summer. Reductions in aqueous buffering capacity and decreases in particle size decrease local sulphur deposition in favour of SO_2 deposition further downwind; a by-product of the NH_3 emissions reduction is to increase the overall transport distance of emitted atmospheric sulphur. Ammonia emissions reductions result in a significant decrease in total ammonia

Base Case – 30% NH3 Emissions   **Base Case – 50% Cdn. Beef Emissio**

Fig. 22. Seasonal average change in PM$_{2.5}$ mass (μg m^{-3}) associated with a 50% reduction in Canadian beef-cattle emissions. Portion of model domain covering provinces of Alberta, Saskatchewan, and Manitoba.

deposition and a smaller decrease in nitrate deposition, in regions of high ammonia emissions.

Figures 10 and 11 show that the impact of NH_3 emissions reductions is highly episodic in nature. In both high and low resolution model runs, 95th percentile values of the differences between base case and scenarios are often much larger (up to a factor of 6) than the median differences of the distribution. This is in accord with the known chemistry of p-NH_4 formation, specifically ammonium nitrate, and our analysis suggests that $PM_{2.5}$ mass decreases resulting from ammonia emissions reductions will result from decreases in particle ammonium and particle. Relatively small changes in local temperature, humidity, and precursor-gas concentrations can give rise to rapid particle formation and/or loss conditions (e.g., Yu et al., 2005). Decreases in NH_3 emissions may have a modest or low impact on $PM_{2.5}$ levels in median or average conditions, but a much larger impact when $PM_{2.5}$ levels are high.

Reductions in NH_3 emissions may result in decreases in acid deposition and in exceedance of S + N critical loads for sensitive Canadian ecosystems. The predicted small changes to sulphur deposition, on the other hand, have little impact on sulphur critical-load exceedances, implying that NH_3 emissions reductions at the current time will not reduce the sulphur acidification of sensitive ecosystems. However, if the ability of these ecosystems to absorb nitrogen becomes saturated, the role of NH_3 on the exceedance of critical loads does become substantial. Ammonia emissions reductions hence may eventually be required to reduce acidification of Canadian ecosystems

The important linkages between transport and chemistry when NH_3 reductions are considered suggests that cross-border transport may be an important factor when assessing the outcomes of NH_3 emission reduction strategies. Ammonia and PM concentrations may be affected considerably downwind, and sulphur and nitrogen transport distances from sources of sulphur and nitrogen and associated deposition patterns are changed. Some future scenario runs should focus on trans-boundary transport.

The beef-cattle emissions scenario shows that the uncertainty associated with the updated 2002 Canadian agricultural NH_3 emissions inventories for this source subsector is large. Future work on emissions inventories should attempt to reduce this uncertainty. This scenario also serves to show the potential for NH_3 emissions reduction scenarios that assess the impacts of agricultural-subsector-specific changes in emitting practices. Scenarios examining the impacts of NH_3 management practice changes should therefore be considered in future work.

A potentially significant source of uncertainty in all of the model results is the role of coarse-mode chemistry in the real atmosphere; the model neglects base cation chemistry (calcium, magnesium, sodium, potassium), and the model particle nitrate formation may therefore be more sensitive to changes in ammonia gas emissions than would occur in the ambient atmosphere. Coarse-mode particle chemistry may reduce the impact of ammonia emissions reductions by competing with the fine mode for the available nitric acid, as well as providing sites for condensation of nitric and sulphuric acid during intense dust storm events. For this reason, the changes depicted here should be considered upper limits. Inclusion of coarse-mode chemistry is recommended for future model simulations of ammonia emission scenarios.

Edited by: S. Pandis

References

Aber, J. D. and Magill, A. H.: Chronic nitrogen additions at the Harvard Forest (USA): the first 15 years of a nitrogen saturation experiment, Forest Ecol. Manage., 196, 1–5, 2004.

Adema, E. H., Heeres, P., and Hulskotte, J.: On the dry deposition of NH_3, SO_2, and NO_2 on wet surfaces in a small scale wind tunnel. edited by: Hartman, H. F., Proceedings of the Seventh World Clean Air Congress, Clean Air Society of Australia and New Zealand, 2, 1–8, 1986.

Anlauf, K. G., Lusis, M. A., and Wiebe, H. A.: Toronto Air Quality Study, Env Canada report ARQA-60-78, 1978.

Ansari, A. S. and Pandis, S. N.: Response of inorganic PM to precursor concentrations, Environmental Science and Technology, 32, 2706–2714, 1998.

Ansari, A. S. and Pandis, S. N. Prediction of multicomponent inorganic atmospheric aerosol behavior, Atmos. Environ., 33, 745–757, 1999.

Ayres, J., Bittman, S., Girdhar, S., Sheppard, S., Niemi, D., Ratté, D., Smith, P.: Chapter 5: Sources of Ammonia Emissions. *In* Environment Canada. The 2008 Canadian Atmospheric Assessment of Agricultural Ammonia, Environment Canada, Gatineau, QC, Canada, in press, 2009.

Binkowski F. S. and Shankar U.: The Regional Particulate Matter Model. 1. Model description and preliminary results, J. Geophys. Res., 100, 26, 191–26, 1995.

Binkowski, F. S. and Roselle S. J.: Models-3 Community Multiscale Air Quality (CMAQ) model aerosol component 1. Model description, J. Geophys. Res. Atmos., 108, AAC 3-1–3-18, 2003.

Bittman, S., Ayres, J., Sheppard, S., and Girdhar, S.: Chapter 4: Emission Inventory Development. *In* Environment Canada, The 2008 Canadian Atmospheric Assessment of Agricultural Ammonia (in press), Environment Canada, Gatineau, QC, Canada, 2008.

Blanchard, C. L., Roth, P. M., Tanenbaum, S. J., Ziman, S. D., and Seinfeld, J. H.: The use of ambient measurements to identify which precursor species limit aerosol formation, J. Air Waste Manage. Assoc., 50, 2073–2084, 2000.

Brosset, C.: Water-soluble sulphur compounds in aerosols, Atmos. Environ., 12, 25–38, 1978.

Carolina Environmental Program (CEP): Sparse Matrix Operator Kernel Emission (SMOKE) modelling system, University of North Carolina, Carolina Environmental Programs, Chapel Hill, NC, online available at: http://www.smoke-model.org/index.cfm, 2003.

Chang, J. S., Brost, R. A., Isaksen, I. S. A., Madronich, S., Middleton, P., Stockwell, W. R., Walcek, C. J.: A three-dimensional Eulerian acid deposition model: Physical concepts and formulation, J. Geophys. Res., 92, 14681–14700, 2003.

Coste, J. H. and Courtier, G. B.: Sulphuric acid as a disperse phase in town air, T. Faraday Soc., 32, 1198–1202, 1936.

Côté, J., Gravel, S., Méthot, A., Patoine, A., Roch, M., and Staniforth, A.: The operational CMC-MRB Global Environmental Multiscale (GEM) model. Part 1: Design considerations and formulation, Mon. Weather Rev., 126, 1373–1395, 1998.

D'Ans, J.: Zur Kenntnis der Suaren Sulfate VII. Sulfate und Pyrosulfate des Natrium, Kalium und Ammonium. Z. Allg. Anorg, On the knowledge of acidic sulphate VII. Acid sulphate and pyro-sulphate of sodium, potassium and ammonium, Journal for Inorganic and General Chemistry Ch., 80, 235–245, 1913.

Denman, K. L., Brasseur, G., Chidthaisong, A., Ciais, P., Cox, P.M., Dickinson, R. E., Hauglustaine, D., Heinze, C., Holland, E., Jacob, D., Lohmann, U., Ramachandran, S., da Silva, P. L., Wofsy, S. C., and Zhang, X. Couplings Between Changes in the Climate System and Biogeochemistry, in: Climate Change 2007: The Physical Science Basis. Contribution of Working Group I to the Fourth Assessment Report of the Intergovernmental Panel on Climate Change edited by: Solomon, S., Qin, D., Manning, M., Chen, Z., Marquis, M., Averyt, K. B., Tignor, M., Miller, H. L., Cambridge University Press, Cambridge, UK and New York, USA, 499–587, 2007.

Dentener, F., Drevet, J., Lamarque, J. F., Bey, I., Eickhout, B., Fiore, A. M., Hauglustaine, D., Horowitz, L. W., Krol, M., Kulshrestha, U. C., Lawrence, M., Galy-Lacaux, C., Rast, S., Shindell, D., Stevenson, D., Van Noije, T., Atherton, C., Bell, N., Bergman, D., Butler, T., Cofala, J., Collins, B., Doherty, R., Ellingsen, K., Galloway, J., Gauss, M., Montanaro, V., Muller, J.-F., Pitari, G., Rodriguez, J., Sanderson, M., Solmon, F., Strahan, S., Schultz, M., Sudo, K., Szopa, S., and Wild, O. Nitrogen and sulfur deposition on regional and global scales: A multimodel evaluation, Global Biogeochem. Cy., 20, GB4003, doi:10.1029/2005GB002672, 2006.

Eder, B. and Yu, S.: A performance evaluation of the 2004 release of Models-3 CMAQ, Atmos. Environ., 40, 4811–4824, 2006.

Erisman, J. W., Vanelzakker, B. G., Mennen, M. G., Hogenkamp, H., Zwart, E., Van den Beld, L., Romer, F. G., Bobbink, R., Heil, G., Raessen, M., Duyzer, J. H., Verhage, H., Wyers, G. P., Otjes, R. P., and Möls, J. J.: The Elspeetsche Veldexperiment on surface exchange of trace gases: summary of results, Atmos. Environ., 28, 487–496, 1994a.

Erisman, J.W., Mennen, M., Hogenkamp, J., Kemkers, E., Godhart, D., van Pul, A., Draaijers, G., Duyzer, J., Wyers, P.: Dry deposition monitoring of SO₂, NH₃ and NO₂ over a coniferous forest, in: Proceedings of EUROTRAC Symposium '94, edited by: Borrell, P. M., Borrell, P., Cvitas, T., and Seiler, W., The Hague, The Netherlands, 655–659, 1994b.

Fenn, R. W., Gerber, H. E., and Wasshuasen, D.. Measurements of the sulphur and ammonium component of the arctic aerosol of the Greenland icecap, J. Atmos. Sci., 20, 466–468, 1963.

Fenn, M. E., Jovan, S., Yuan, F., Geiser, L., Meixner, T., and Gimeno, B. S.: Empirical and simulated critical loads for nitrogen deposition in California mixed conifer forests, Environ. Poll., 155, 492–511, 2008.

Fowler, D., Cape, J. N., Coyle, M., Smith, R. I., Hjellbrekke, A.-G., Simpson, D., Derwent, R. G., and Johnson, C. E.: Modelling photochemical oxidant formation, transport, deposition and exposure of terrestrial ecosystems, Environ. Poll., 100, 43–55, 1998.

Fung, C. S., Misra, P. K., Bloxam, R., and Wong, S.: A numerical experiment on the relative importance of H₂O₂ and O₃ in aqueous conversion of SO₂ to SO₄, Atmos. Environ., 25A, 411–423, 1991.

Gilliland, A. B., Appel, K. W., Pinder, R. W., and Dennis, R. L.: Seasonal NH₃ emissions for the continental United States: inverse model estimation and evaluation, Atmos. Environ., 40, 4986–4998, 2006.

Gong, W., Dastoor, A. P., Bouchet, V. S., Gong, S., Makar, P. A., Moran, M. D., Pabla, B., Ménard, S., Crevier, L.-P., Cousineau, S., and Venkatesh, S.: Cloud processing of gases and aerosols in a regional air quality model (AURAMS), Atmos. Res., 82, 248–275, 2006.

Gordon, R. J. and Bryan, R. J.: Ammonium nitrate in airborne particles in Los Angeles, Environmental Science and Technology, 7, 645–647, 1973.

Hall, J., Hornung, M., Kennedy, F., Langan, S., Reynolds, B., and Aherne, J.: Investigating the uncertainties in the simple mass balance equation for acidity critical loads for terrestrial ecosystems. Water Air Soil Pollut. Focus, 1, 43–56, 2001.

Heard, M. J. and Wiffen, R. D.: Electron microscopy of natural aerosols and the identification of particulate ammonium sulphate, Atmos. Environ., 3, 337-340, 1969.

Herrmann, H., Ervens, B., Jacobi, H.-W., Wolke, R., Nowack, P., and Zellner, R.: CAPRAM2.3: A Chemical Aqueous Phase Radical Chemistry for Tropospheric Chemistry, J. Atmos. Chem., 36, 231–284, 2000.

Herrmann, H., Tilgner, A., Barzaghi, P., Majdik, Z., Gligorovski, S., Poulain, L., and Monod, A.: Towards a more detailed description of tropospheric aqueous phase organic chemistry: CAPRAM 3.0., Atmos. Environ., 39, 4351–4363, 2005.

Houyoux, M. R., Vukovich, J. M., Coats, C. J. Jr., and Wheeler, N. J. M.: Emission inventory development and processing for the Seasonal Model for Regional Air Quality (SMRAQ) project, J. Geophys. Res., 105, 9079–9090, 2000.

Jeffries, D. S. and Ouimet, R.: Critical loads: are they being exceeded? [In] Chapter 8 of Canadian Acid Deposition Science Assessment 2004, Environment Canada, 4905 Dufferin Street, Downsview, Canada, 440 pp., online available at: http://www.msc-smc.ec.gc.ca/saib/acid/acid_e.html, 2005.

Jeffries, D. S., Lam, D. C. L., Moran, M. D., and Wong, I.: The effect of SO₂ emission controls on critical load exceedances for lakes in southeastern Canada, Water Sci. Tech., 39, 165–171, 1999.

Junge, C. E. and Ryan, T. G.: Study of the SO2 oxidation in solution and its role in atmospheric chemistry, Q. J. Roy. Meteor. Soc., 84, 46–55, 1958.

Kaste, Ø, Henriksen, A., and Posch, M.: Present and potential nitrogen outputs from Norwegian soft water lakes – an assessment made by applying the steady-state First-order Acidity Balance

(FAB) model, *Hydrol. Earth Syst. Sci.*, 6, 101–112, 2002.

Kusik, C. L. and Meissner, H. P.: Electrolyte activity coefficients in inorganic processing, A.I.Ch.E. Symposium 173, 14–20, 1978.

Logan, J. A.: An analysis of ozonesonde data for the troposphere: Recommendations for testing 3-D models, and development of a gridded climatology for tropospheric ozone, J. Geophys. Res., 104, 16115–16149, 1998.

Luo, C., Zender, C. S., Bian, H., and Metzger, S.: Role of ammonia chemistry and coarse mode aerosols in global climatological inorganic aerosol distributions, Atmos. Environ., 41, 2510–2533, 2007.

MacDonald, A. M., Anlauf, K. G., Leaitch, W. R., and Liu, P. S.: Multi-year Chemistry of Particles and Selected Trace Gases at the Whistler High Elevation Site, EOS Trans., AGU 87(52), Fall Meet., Suppl., Abstract A53b-0179, 2006.

Makar, P. A., Bouchet, V. S., and Nenes, A.: Inorganic chemistry calculations using HETV – a vectorized solver for the SO_4^{2-}-NO_3^- -NH_4^+ system based on the ISORROPIA algorithms, Atmos. Environ., 37, 2279–2294, 2003.

Mathur, R. and Dennis, R. L.: Seasonal and annual modeling of reduced nitrogen compounds over the eastern United States: Emissions, ambient levels, and deposition amounts, J. Geophys. Res. Atmos., 108, ACH 22-1–ACH 22-19 2003.

McNulty, S. G., Cohen, E. C., Moore Myers, J. A., Sullivan, T. J., and Li, H.: Estimates of critical acid loads and exceedances for forest soils across the conterminous United States, Environ. Pollut., 149, 281–292, 2007.

Moran, M. D., Zheng, Q., Samaali, M., Narayan, J., Pavlovic, R., Cousineau, S., Bouchet, V. S., Sassi, M., Makar, P. A., Gong, W., Gong, S., Stroud, C., and Duhamel, A.: Comprehensive surface-based performance evaluation of a size-and composition-resolved regional particulate-matter model for a one-year simulation. Proc. 29th NATO/SPS ITM on Air Pollution Modelling and Its Application, Aveiro, Portugal, 24–28 Sept., 9 pp., published in Air Pollution Modeling and its Application XIX, 2008, edited by: Borrego, C. and Miranda, A. I., Springer, Dordrecht, The Netherlands, 434–442, 2007.

Moran, M. D., Zheng, Q., Pavlovic, R., Cousineau, S., Bouchet, V. S., Sassi, M., Makar, P. A., Gong, W., and Stroud, C.: Predicted acid deposition critical-load exceedances across Canada from a one-year simulation with a regional particulate-matter model. Proc. 15th Joint AMS/A&WMA Conf. on Applications of Air Pollution Meteorology, 21–24 January, New Orleans, American Meteorological Society, Boston, 20 pp., online available at: http://ams.confex.com/ams/pdfpapers/132916.pdf, 2008.

Neirynck, J., Kowalski, A. S., Carrara, A., Ceulemans, R.: Driving forces for ammonia fluxes over mixed forest subjected to high deposition loads, Atmos. Environ., 39, 5013–5024, 2005.

Pinder, R. W., Adams, P. J., and Pandis, S. N.: Ammonia emission controls as a costeffective strategy for reducing atmospheric particulate matter in the eastern United States, Environ. Sci. Technol., 41, 380–386, 2007.

Phillips, S. B., Aneja, V. P., Kang, D., and Arya, S. P.: Modelling and analysis of the atmospheric nitrogen deposition in North Carolina, International Journal of Global Environmental Issues, 6, 231–252, 2006.

Pinder, R. W., Gilliland, A. B., and Dennis, R. L.: Environmental impact of atmospheric NH3 emissions under present and future conditions in the eastern United States, Geophys. Res. Lett., 35,

L12808, doi:10.1029/2008GL033732, 2008.

Quan, J. and Zhang, X.: Assessing the role of ammonia in sulfur transformation and deposition in China, Atmos. Res., 88, 78–88, 2008.

Robbins, R. C. and Cadle, R. D.: Kinetics of the reaction between gaseous ammonia and sulfuric acid droplets in an aerosol, J. Phys. Chem., 62, 469–471, 1958.

Schwarze, P. E., Orevik, J., Lag, M., Refsnes, M., Nafstad, P., Hetland, R. B., and Dybing, E.: Particulate matter properties and health effects: Consistency of epidemiological and toxicological studies, Human and Experimental Toxicology, 25, 559–579, 2006.

Scire, J. S., Lurmann, F. W., Karamchandani, P., Venkatram, A., Yamartino, R., Young, J., and Pleim, J.: ADOM/TADAP Model Development Program, Volume 9: User's Guide, Environmental Research and Technology, Inc., Newbury Park, California, USA, 1986.

Seinfeld, J. H. and Pandis, S. N.: Atmospheric chemistry and physics: from air pollution to climate change, John Wiley and Sons, Inc., New York, USA, 1326 pp., 1998.

Spranger, T., Hettelingh, J.-P., Slootweg, J., Posch, M.: Modelling and mapping long-term risks due to reactive nitrogen effects: An overview of LRTAP convention activities, Environ. Pollut., 154, 482–487, 2008.

Spurny, K. and Heard, M. J.: Discussions: Electron microscopy of natural aerosols and the identification of particulate ammonium sulphate. Atmos. Environ., 3, 483, 1969.

Stelson, A. W., Friedlander, S. K. and Seinfeld, J. H.: A note on the equilibrium relationship between ammonia and nitric acid and particulate ammonium nitrate, Atmos. Environ., 13, 369–371, 1979.

Stilg, M.: World-wide limits for toxic and hazardous chemicals. Noyes Publications, NJ, USA, 792 pp., 1994.

Stockwell, W. R. and Calvert, J. G.: The mechanism of the HO-SO2 reaction, Atmos. Environ., 17, 2231–2235, 1983.

Sutton, M. A., Asman, W. A. H., SchjoØrring, J. K.: Dry deposition of reduced nitrogen, Tellus 46, 255–273, 1994.

Tanner, R. L.: An ambient experimental study of phase equilibrium in the atmospheric system: aerosol H^+, NH_4^+, SO_4^{2-}, NO_3^-, $NH_3(g)$, $HNO_3(g)$, Atmos. Environ., 16, 2935–2942, 1983.

Tsimpidi, A. P., Karydis, V. A., and Pandis, S. N.: Response of Inorganic Fine Particulate Matter to Emission Changes of Sulfur Dioxide and Ammonia: The Eastern United States as a Case Study, J. Air Waste Manage. Assoc., 57, 1489–1498, 2007.

Van Hove, L. W. A., Adema, E. H., Vredenberg, W. H., and Pieters, G. A.: A study of the adsorption of NH3 and SO2 on leaf surfaces. Atmos. Environ., 23, 1479–1486, 1989.

Venkatram, A. and Karamchandani, P. K.: Testing a comprehensive acid deposition model. Atmospheric Environment, 22, 737–747, 1988.

Wang, J., Deeter, M. N., Gille, J. C., and Bailey, P. L.: Retrieval of tropospheric carbon monoxide profiles from MOPITT: Algorithm description and retrieval simulation, Proc. SPIE – Int. Soc. Opt. Eng., 3756, 437–446, 1999.

Wang, Z., Xie, F., Sakurai, T., Ueda, H., Han, Z., Carmichael, G. R., Streets, D., Engardt, M., Holloway, T., Hayami, H., Kajino, M., Thongboonchoo, N., Bennet, C., Park, S. U., Fung, C., Chang, A., Sartelet, K., and Amann, M.: MICS-Asia II: Model intercomparison and evaluation of acid deposition, Atmos. Environ.,

42, 3528–3542, 2008.

West, J. J., Ansari, A. S., and Pandis, S. N.: Marginal $PM_{2.5}$: Nonlinear aerosol mass response to sulfate reductions in the eastern United States, J. Air Waste Manage. Assoc., 49, 1415–1424, 1999.

Wright, R. F., Alewell, C., Cullen, J. M., Evans, C. D., Marchetto, A., Moldan, F., Prechtel, A., and Rogora, M.: Trends in nitrogen deposition and leaching in acid-sensitive streams in Europe, Hydrol. Earth Syst. Sci., 5, 299–310, 2001,
http://www.hydrol-earth-syst-sci.net/5/299/2001/.

Ying, Q. and Kleeman, M. J.: Source contributions to the regional distribution of secondary particulate matter in California. Atmos. Environ., 40, 736–752, 2006.

Yu, S., Dennis, R., Roselle, S., Nenes, A., Walker, J., Eder, B., Schere, K., Swall, J., and Robarge, W.: An assessment of the ability of three-dimensional air quality models with current thermodynamic equilibrium models to predict aerosol NO_3^-. J. Geophys. Res., 110, doi:10.1029/2004JD004718, 22 pp., 2005.

Zhang, L., Gong, S., Padro, J., and Barrie, L.: A size-segregated particle dry deposition scheme for an atmospheric aerosol module. Atmos. Environ., 35, 549–560, 2001.

Zhang, L., Moran, M. D., Makar, P. A., Brook, J. R., and Gong, S.: Modelling gaseous dry deposition in AURAMS: a unified regional air-quality modelling system. Atmos. Environ., 36, 537–560, 2002.